ELSEVIER

Coordination Chemistry Reviews
190–192 (1999) 405–445

COORDINATION CHEMISTRY REVIEWS

www.elsevier.com/locate/ccr

Isokinetic and isoequilibrium relationships in spin–crossover systems☆

Wolfgang Linert [a,*], Andrei B. Kudryavtsev [b]

[a] *Institute of Inorganic Chemistry, Vienna University of Technology, Getreidemarkt 9, A-1060 Vienna, Austria*

[b] *D. Mendeleev University of Chemical Technology of Russia, Miusskaya sq. 9, 125047, Moscow, Russia*

Accepted 13 March 1999

Contents

☆ We wish to dedicate this paper in memorial to our late friend and mentor Viktor Gutmann who passed away in July 1998.

* Corresponding author. Tel.: +43-1-58880115350; fax: +43-1-5880115399.
E-mail address: wlinert@mail.zserv.tuwien.ac.at (W. Linert)

0010-8545/99/$ - see front matter
PII: S0010-8545(99)00097-1

Abstract

The theory of the isokinetic relationship (IKR, sometimes referred to as compensation effect) and its connection to generalised linear free energy relationships and its application to systems exhibiting spin–crossover both in solid state and in solution is reviewed. A theoretical background to the occurrence of the IKR is given in analogy to chemical reactions without spin-state transformations. Applications of the relationships are suggested on the basis of detecting changes in reaction pathways of the spin-state changes within a given series of reactions.

Keywords: Isokinetic relationship; Line or free energy relationships (LFER); Spin-state changes; Spin–crossover systems

1. Introduction

One of the greatest successes of the crystal field theory, was the description of magnetic properties of coordination compounds based on the idea of competition between the states with paired and unpaired electrons on the available energy levels split by the crystal field. When crystal field splitting of d-levels is much higher or much lower than the energy of electron repulsion (pairing energy) the Low Spin (diamagnetic) and High Spin (paramagnetic) states are realised. There are, however, also a (relatively small) number of complexes corresponding to approximate equality of the energies of HS and LS states which makes the population of both in a certain temperature range possible. They are known by the name 'spin–crossover compounds'. Thermally induced spin–crossover, i.e. a transition from LS and HS states due to the changes in their population with temperature, can only be observed when the ground state is the LS state. This condition arises from the fact that the degeneracy of the HS state is higher than that of the LS state. This makes the entropy of transition LS → HS positive, and such a transition can only be observed (at positive absolute temperatures) when E_{HS} is higher than E_{LS}. The molecules with HS ground state cannot be converted into LS complexes by heating, even if the excited LS state lies several kT above the HS state. Such transitions are however, accessible non-thermally, e.g. via excitation of a molecule by light into higher excited states and subsequent (radiationless) relaxation into the LS state. The LS–HS transitions can also be activated by light and if performed at sufficiently low temperatures result in long-living metastable HS states (LIESST-effect) as well as by a change of the nature of atomic nucleus due to the nuclear decay (NIESST). These effects are of great importance, both in fundamental and applied research, and they are being widely investigated [1–3].

Spin–crossover can be observed both in solid state [4–7] and in solutions [8–15] (where, however, solvolysis, [9,10,14] ligand- and anion-exchange reactions, [10] and complex deprotonation [13], complicate the situation). The most interesting results have been, up to now, obtained in solid state, where a variety of different shapes of temperature dependencies of magnetic susceptibility has been observed and successfully interpreted using the model of regular solutions, i.e. taking into account the influence of the surrounding on the state of a given spin–crossover unit. In non-diluted solid state systems the presence of HS or LS complexes in the nearest neighbourhood of the considered particle, affect its free energy which results in 'steep' or 'abrupt' spin–crossover accompanied sometimes, by hysteresis indicating the separation of HS and LS phases. The parameter determining these modes of spin–crossover is the interaction term (Γ), identical [16] to the free energy of exchange in the theory of solutions. As can be expected, the shape of spin–crossover curves is dependent of the counter-ions, solvate molecules in crystal–solvates and on the substituents in the ligands as determining the surrounding electron distribution of a spin–crossover unit.

In diluted solid systems (mixed Fe–Zn complexes for example [17]) and in liquid solutions, the observed spin–crossover curves (a gradual spin–crossover) correspond to zero exchange free energy, i.e. to the case of ideal solutions. The observed variations in magnetic behaviour in these systems are due to the variation in the donor and acceptor properties of the ligand (inner sphere effect), solvation by solvent molecules (outer-sphere and inner-sphere effects) and/or association with counter-ion.

There are also examples of LS–HS transitions in coordination compounds connected with the changes in the symmetry type of the complex. For example, 4-fold coordinated complexes of Ni(II) appear often in equilibria between square–planar (diamagnetic) and tetrahedral (paramagnetic) conformations. The standard enthalpy of the transition from square–planar to tetrahedral conformations in a series of complexes of Ni(II) is small and positive (0–5 kcal mol^{-1} [18]). These complexes behave, therefore, formally as conventional spin–crossover compounds with HS state populated at higher temperatures. However, this is not a thermally induced spin–crossover because, by changing temperature we do not populate excited states but change the 'average degeneracy' of the ground state of a molecule. Furthermore, square–planar complexes of Ni(II) can coordinate additional donor molecules, which yields paramagnetic octahedral complexes of Ni(II). The standard enthalpy of this reaction for bis-salicylaldoximato Nickel(II) [19a] is negative (-13.5 kcal mol^{-1}) and at higher temperatures the LS state is more populated. However, this is the result of decreasing the number of molecules (due to the dissociation of solvates) with paramagnetic ground state and not of the population of the exited state.

Another example of solvation-induced spin–crossover, is the equilibrium between a square–planar mixed ligand (diamino-β-diketonato)Ni(II) complex and its octahedral and five-coordinated solvates [20,21], which will be considered in Section 7 of this review.

The intensely studied spin–crossover in complexes with photo-isomerisable ligands [22] should be considered as belonging to this class of transitions that are different from thermally induced (conventional) spin–crossover.

Parameters of spin–crossover equilibria:

$$LS \Leftrightarrow HS \tag{1.1}$$

may be determined from electronic (UV–vis) spectra (spin–crossover is usually accompanied by a spectacular change in the colour of the compound), vibrational (IR and Far-IR) spectra, Moessbauer spectra, or from magnetochemical measurements. In the latter case, the calculations are based on the additivity of the magnetic susceptibility:

$$\chi_{obs} = (N\mu_B^2/3kT)\ \mu_{obs}^2 = (N\mu_B^2/3kT)(x_{LS}\mu_{LS}^2 + x_{HS}\mu_{HS}^2) \tag{1.2}$$

where x_{LS} and x_{HS} are molar fractions of LS and HS states, respectively. The fraction of HS state is connected with the equilibrium constant of (Eq. (1.1)) as:

$$x_{HS} = K/(K+1) \tag{1.3}$$

In theory, this expression (the law of mass action) is valid for reactions in ideal crystals or ideal solutions. In practice, it is applicable to diluted solutions both in liquid and solid state. The value of the experimental obtained magnetic moment:

$$\mu_{obs}^2 = (3k/N\mu_B^2)\ T\chi = (31.38 \times 10^{-16}/6.02 \times 10^{23}\ 0.927 \times 10^{-40})\ \chi T$$
$$= 8.002\ \chi_{obs} T \tag{1.4}$$

may be expressed by the magnetic moments of HS and LS states and the equilibrium constant:

$$\mu_{obs}^2 = x_{HS}\mu_{HS}^2 + (1 - x_{HS})\ \mu_{LS}^2 = \mu_{LS}^2 + (\mu_{HS}^2 - \mu_{LS}^2)\ x_{HS}$$
$$= \mu_{LS}^2 + (\mu_{HS}^2 - \mu_{LS}^2)K/(1+K) \tag{1.5}$$

Using this equation it is possible to estimate K from the observed value of magnetic moment if the values μ_{HS} and μ_{LS} are known:

$$K = (\mu_{obs}^2 - \mu_{LS}^2)/(\mu_{HS}^2 - \mu_{obs}^2) \tag{1.6}$$

The magnetic moment corresponding to $^1A_1$ (LS) state may be assumed as approximately zero. The value $\mu_{LS} = (0.3–0.5)\ \mu_B$ commonly used in calculations, takes the contribution from temperature independent paramagnetism into account. The magnetic moment of $^5T_2$ (HS) state depends on the splitting of this term by spin-orbit coupling and axial field distortions. In regular octahedral complexes the magnetic moment of the HS state of Fe(II) complexes varies between the pure spin value 4.9 μ_B at low temperatures, and 5.5 μ_B at room temperature. Using the mean value $5.2\mu_B$ for HS, and $0.3\mu_B$ for LS, makes it possible to get just a rough estimate of spin–crossover equilibrium constant. The actual value of μ_{HS} cannot be determined by extrapolation of the observed temperature dependence of μ to infinitely high temperatures, because the corresponding value is not exactly μ_{HS} [2]. Temperature dependence of μ_{HS} must also be taken into account (see below). In general, a nonlinear regression procedure must be applied to magnetochemical data in order

to obtain estimates of K and μ_{HS} rather than obtaining them from a van't Hoff plot.

2. Isokinetic and isoequilibrium relationships

Both IKR and IER have been reviewed before [23,24]. However, the most important point will be given below to allow straightforward application to the above mentioned spin–crossover systems.

IKR and IR have turned out to be of high applicability in the investigation of similarities and differences in the chemical reactivity within series of reactions, both from the thermodynamic and the kinetic point of view [25]. This especially concerns the reaction series where the variation of temperature is of importance, such as the above mentioned spin–crossover equilibria.

Information concerning substituent and solvent effects on chemical reactivity alone (i.e. without temperature variation) can be correlated in a variety of ways, for example by means of the Hammett relationship [26], Brønsted relationships [27] or correlations of equilibrium and rate constants with solvent parameters such as donor or acceptor numbers [28] or Reichardt's E_T values [29]. Such relationships fall into the large class of linear free energy relationships (LFERs). Broadly speaking, LFERs are produced when rate constants or equilibrium constants (or related functions describing kinetic or thermodynamic chemical behaviour) of a series of reactions are plotted versus a characteristic quantity measured by means of another reaction series [30–32].

In general, LFERs require equilibrium systems associated with Boltzmann distributions of the respective species. It implies that van't Hoff plots ($\ln K$ vs. $1/T$) or for kinetic systems, Arrhenius plots ($\ln k$ vs. $1/T$) must be linear. In fact, this rule only holds for temperature independent enthalpy of reaction or activation, i.e. in the cases when corresponding differences in specific heat are zero. As it will be described below, this is not necessarily the case for spin-state equilibria both in solid state and in solution. In some cases, therefore, nonlinear free energy relationships (NLFER) must be involved.

Whenever a LFER is found, some quantity must be present, which appears in the same functional form in both the 'test reaction series' and the 'reference reaction series'. In what follows this parameter will be given the symbol ξ. So long as only one parameter appears, it may always be expressed in the form of a linear relationship. Furthermore, since thermodynamic functions will be concerned to some extent, the abbreviation x for $1/RT$ will be used. Wherever it is not necessary to distinguish between rate constants and equilibrium constants, both will be referred to as K (Fig. 1):

$$\text{van't Hoff: } \ln K = -\Delta G/RT = -\Delta H/RT + \Delta S/R \tag{2.1}$$

$$\text{Arrhenius: } \ln k = -\Delta H^{\#}/RT + \Delta S^{\#}/R = -E_a/RT + \ln A \tag{2.1a}$$

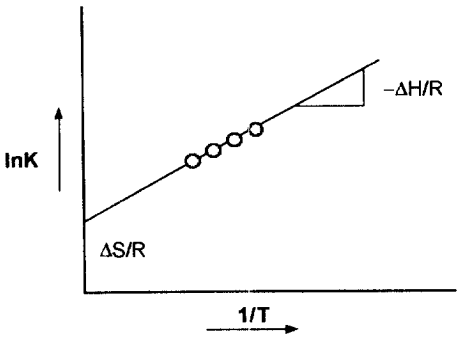

Fig. 1. Schematic van't Hoff plot. Arrhenius plots ($\ln K$ vs. $1/T$) correspond to negative $\Delta H^{\neq}$.

Isokinetic behaviour is found [32] for reaction series in which only one reaction mechanism is followed and, in fact, this is a necessary condition for the occurrence of an LFER described by not more than one parameter ξ. This produces in turn, a common point of intersection of the Arrhenius lines or of the van't Hoff lines ($\ln K$ vs. $x = 1/T$) (Fig. 2). These are called the isokinetic and isoequilibrium

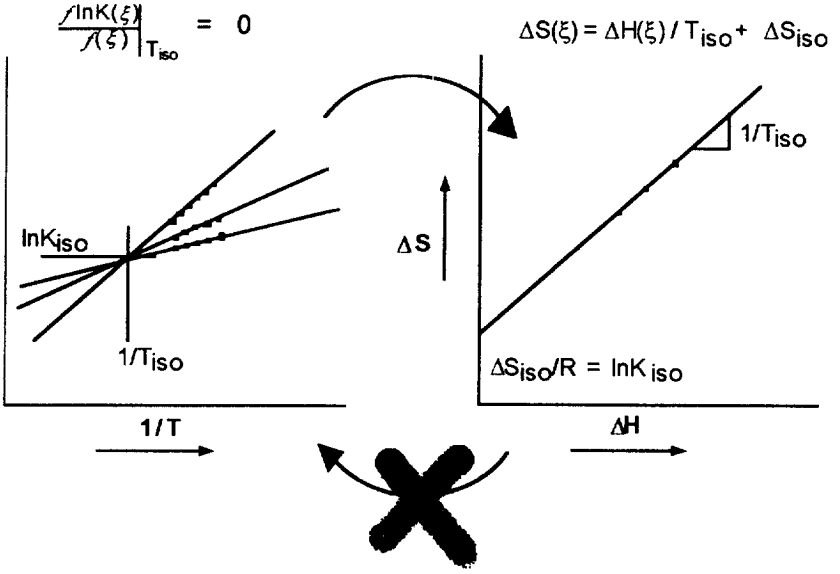

Fig. 2. Left hand side: common point of intersection found for the van't Hoff plots of three reactions belonging to one reaction series (IER, for Arrhenius lines this would correspond to an IKR). Right hand side: linear relationship between entropic and enthalpic contributions to the reactions from the left hand side. If the common point of intersection can be shown with statistical significance, the right hand side can be taken as being implied. However, the reverse argument cannot be granted, because the right hand linear plot might be an artefact without actual physical significance and without implying a common point of intersection at the left hand side.

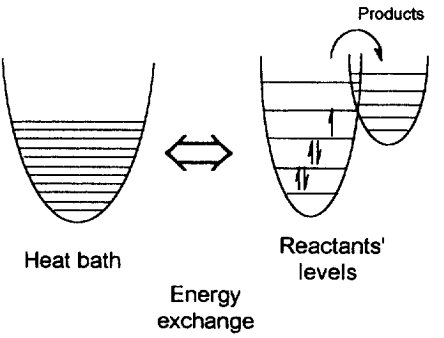

Fig. 3. Reactants distributed in a potential well with a point of no return (i.e. a reaction barrier) coupled to a heat-bath storing energy in vibrational levels.

relationships (IKR and IER), respectively. It appears to be of importance to stress that IKR and IER are to be clearly separated, one being a relationship between kinetic data, the other referring to thermodynamic equilibria. Although their interrelation exists, they should not be treated as being one and the same effect[1].

This effect has also been often referred to as the 'compensation effect'. However, the latter usually means a proportionality between enthalpic and entropic contributions to K which may occur as an artefact [32,33].

Such common points of intersection are also found when the same set of data is depicted for different temperatures in LFER plots. Whereas in the case of the IKR the characteristic intersection abscissa has the dimension of a reciprocal temperature ($x_{iso} = 1/T_{iso}$, where T_{iso} is referred to as the isokinetic temperature), in the latter case a characteristic LFER parameter (ξ_{iso}) is found.

In the following, some general properties of these relationships will be explored and then applied to some actual experimental reaction series (involving both substituent and solvent effects) in order to illustrate the practical value of these concepts.

2.1. Stochastic modelling of IKRs

In Kramer's theory [34] of rate constants, the reactant molecules are supposed to become activated through their collision with other molecules of the surrounding medium, which acts as a constant-temperature 'heat-bath'. After a random walk over discrete energy levels of the reactants they reach the highest point of the

[1] Quite often, no distinction is made between IKR and IER and the van't Hoff plots are miscalled Arrhenius plots. It is a misleading practice, because a pseudo-equilibrium transition state model of chemical reaction involves an unstable and mostly fictitious transition state, whilst in equilibria the participants are stable molecules in their ground states. Also, Arrhenius plots always have negative slopes whilst van't Hoff plots could be directed both downwards and upwards. The IER may be interpreted as IKR being applied to the direct and reverse reactions of an equilibrium (as far as the dynamic interpretation of equilibrium is allowed).

barrier, a point of no return. The crossing over this barrier constitutes the chemical reaction rate. Figs. 2 and 3 and Eq. (2.2) explain this in some detail:

$$d\sigma_l(t)/dt = Z\Bigg[-\sum_{l<m} P_{ml}N^- \sigma_l(t) + \sum_{l<m} P_{ml}N^+_{ml}\sigma_l(t) + \sum_{m<l} P_{lm}N^+_{lm}\sigma_m(t) + \sum_{m>l} P_{lm}N^-\sigma_m(t)\Bigg] \tag{2.2}$$

Here, σ_l represents the time-dependent density of the reactants to the discrete levels l. The P_{lm} are the transition probabilities per collision for the transition from m to l (with $P_{0,-1}=0$), Z is the collision number and N^+_{lm} are the concentration of heat bath molecules which have 'sufficient energy' to excite a molecule from a given level l to a higher level m ($m>l$) and N^- is the concentration of heat-bath molecules able to de-excite a reactant molecule from m to l (m, l).

In the limit of long times, equilibrium should be reached as represented by:

$$d\sigma_l(t)/dt = 0 \tag{2.3}$$

This yields the condition:

$$N_{lm} = \exp(\Delta E/kT)N_{ml} \tag{2.4}$$

which (with ΔE representing the energy difference between two heat-bath energy levels) represents a Boltzmann distribution for the heat-bath. Non-equilibrium approach is to be applied to the reactant distribution, providing that reactants are able to exchange energy with their molecular surroundings.

Eq. (2.2) can be rewritten in the form of a Langevin equation, by assuming l to be continuous and therefore, allowing for a change from a difference equation to a differential equation, namely:

$$\frac{\partial\sigma(t)}{\partial t} = \frac{\partial}{\partial l}R(l)\left[\frac{\partial\sigma}{\partial l} + \frac{1}{k_B T}h\frac{\partial}{\partial l}\omega(l)\sigma\right] + g(l) \tag{2.5}$$

Here, $g(l)$ represents a source term for particles, so that a steady-state solution of the master equation (Eq. (2.5)) can be obtained under the condition of large barriers with a point of no return at the energy barrier, and connected with a surrounding heat-bath. It has been assumed that during a reaction a non-equilibrium steady-state distribution of reactant particles is present, so that the solution of the differential equation (Eq. (2.5)) takes the form [34–37]:

$$k = \phi(s_N)\left\{\int_0^{s_N} dl \exp\left(-\frac{h}{RT}\int_0^l \omega(l'')dl''\right)\int_0^{s_N} dl' \frac{\exp\left(\frac{1}{RT}\int_0^{s_N}\omega(l'')dl''\right)}{P(l')}\phi(l')\right\} \tag{2.6}$$

This integral may be solved by partial integration and thereupon yields, assuming that the energy barrier is much larger than kT, the following simplified form:

$$k \cong A_0(h\omega/kT)P_{s_N,s_{N-1}}\exp(-s_N h\omega/kT) \tag{2.7}$$

The terms A_o, $s_N h\omega$, T and $P_{s_N, s_{N-1}}$ represent a constant involving mainly the collision number, the energy barrier height, and the temperature of the molecular surroundings of the reactants (i.e. the heat-bath) and the quantum-mechanical transition-probability of a transition between the reactant level s_{N-1} and the highest reactant level (i.e. the point of no return) s_N, respectively.

The problem of understanding the IKR is at this point transferred to the problem of the quantum-mechanical transition probability $P_{s_N, s_{N-1}}$ [38]. When using, like McCoy [36], or earlier Kramers [34], the Landau–Teller transition probabilities [39] which are based on a translational energy exchange between a non-vibrating particle (i.e. a member of the heat-bath) and an harmonic vibrator, isoentropic behaviour is found. In condensed phases, however, it must be assumed that the heat-bath mainly contains energy stored in the form of vibrational degrees of freedom. This situation refers to that given in Fig. 3. Note that the (molecular) structure of the heat-bath is not included in its required properties.

The appropriate transition probabilities for a vibrational–vibrational energy transfer are calculated in [38] and shown to yield:

$$P_{lm} = l \exp(\omega/v) \tag{2.8}$$

where a resonance condition of the form:

$$vm = \omega l \tag{2.9}$$

is included, meaning that energy is exchanged with the highest probability at equal energies (m represents the number of the heat-bath level, v the associated frequency, and the resonance condition is given in its form for harmonic oscillator; ω, l refer to the respective parameters of the reactant system.) Using this, the following form of the rate constant is found:

$$k = A_o s_N (h\omega/k_B T_{exp})^2 \exp[-s_N(\omega/v - h\omega/k_B T_{exp})] \tag{2.10}$$

Here v represents a vibrational heat-bath frequency predominantly active in the energy exchange with the reactants. From this, the IKR follows immediately.

Formally, IKR or IER corresponds to the condition:

$$\left.\frac{\partial \ln k(\xi)}{\partial \xi}\right|_{1/T_{iso}} = 0 \tag{2.11}$$

manifesting that in the isokinetic point rate or equilibrium constant does not depend on the variable parameter ξ. If, for example, we consider the reactants, the parameter ξ from Eq. (2.11) may be identified with the frequency ω of vibrations along the reaction coordinate. Then:

$$[\partial \ln K(\omega)/\partial\omega]_{T_{iso}} = 0 \tag{2.11a}$$

Applying this condition to Eq. (2.4), a relationship is found between T_{iso} and the vibrational frequency predominantly exchanging energy with the reactants present in their molecular surroundings:

$$1/RT_{iso} = 1/E + 1/N_L h\nu \tag{2.12}$$

where h = Planck's constant; N_L = Avogadro's number; k_B = Boltzmann's constant; and ν = the predominantly active heat-bath frequency. The first right-hand term is associated with collision activation and may be neglected for reaction series in condensed phase, where vibrational activation is predominant. In this case:

$$1/RT_{iso} = 1/N_L h\nu \tag{2.13}$$

should be valid. This means that, in whatever form the members of the series are represented, they exhibit the same rate at T_{iso} or show a minimum in selectivity at this temperature. It might be significant for this approximation that in the gas phase, where the energy exchange occurs by individual collisions, the experimental results show $1/T_{iso}$ values near zero, i.e. isoentropic behaviour is observed. At T_{iso}, the dependence upon ξ vanishes from the rate equations and the members of the reaction series cannot therefore be identified by means of their rate constants, i.e. they exhibit iso-selective behaviour. It should be pointed out that the relationship (Eq. (2.13)) has been shown to be valid for a large number of reaction series in solution. The characteristic frequency can be found in the Far-IR spectra of the solvents used in the respective IKR [40]. Obviously, the given theoretical description might be applied to spin–crossover dynamics, as long as the potential surfaces do not change significantly and as long as $E_a > kT$ a requirement which might become important with tunnelling processes.

2.2. Negative isokinetic temperatures

There are, in the literature, several examples of statistically significant negative T_{iso} values, for example the ionisation constants of substituted benzoic acids [40–43]. Obviously such a T_{iso} cannot be related to a frequency of vibration as is required by a theory such as that outlined above. The first point to be made is that these theories have all been developed for elementary steps and a negative isokinetic temperature bears a similar relationship to these theories as does a calculated negative energy of activation to, say, collision theory. In fact, whenever the extrapolation of Arrhenius or van't Hoff lines yields a negative T_{iso}, one might visualise the situation in terms of the slope of the ΔH versus ΔS plot, since negative values of T_{iso} are then readily accommodated in the framework of anti-compensation, i.e. ΔH and ΔS are shifted in opposite directions within the considered reaction series (known as 'anticompensation'). However, for IKRs negative T_{iso} values can be explained in terms of processes that can be dissected into two steps, one of which more strongly affects the overall energy, and the other the overall entropy, with both steps affected in opposite sense by varying reactants or substrata.

3. Isokinetic relationships in spin–crossover dynamics

The HS → LS relaxation kinetics in solutions of Fe complexes in polar solvents have been studied by Hendrickson and co-workers [44]. The complexes were of

hexadentate Schiff base condensate of varying numbers of moles of different aldehydes (6-methyl-2-pyridinecarboxaldehyde: Mepy, and 2-pyridinecarboxaldehyde: Py) and amine (tris(2-aminoethyl)amine: tren). This ligand provides therefore, for the ligand-defined variations within the first coordination sphere of Fe. Three types of kinetic spin–crossover correlations of have been investigated: correlations of activation parameters with first coordination sphere composition, solvent and concentration of complex in solution.

A quite good IKR is observed for the variations in the composition of first coordination sphere, of complexes derived from $[Fe(Py)_3tren]^{2+}$ ($T_{iso} \approx 300$ K, Fig. 4). Acetone shows some weak absorptions around 200 cm^{-1} which might be assigned to the heat-bath frequencies according to Eq. (2.13).

The variations in concentration of $[Fe(Py)_3tren]^{2+}$ in acetone solution is also accompanied by an apparent IKR ($T_{iso} \approx 230$ K, Fig. 5). Obviously the above theory does not account for effects due to concentration variation. However, the reaction coordinate of spin–crossover transitions is associated with the metal–N stretching vibrations (some authors also suggest a contribution from torsional modes [45]) occurring in the first coordination sphere. In this case, the low-temperature tunnelling does not play a significant role because the experimental data do not show any curvature of Arrhenius plots in the low temperature region[2]. The influence of concentration was explained as proceeding from ion association, which may change the crystal field strength (about 300 cm^{-1} would account for the observed effect) and/or vibrational mass.

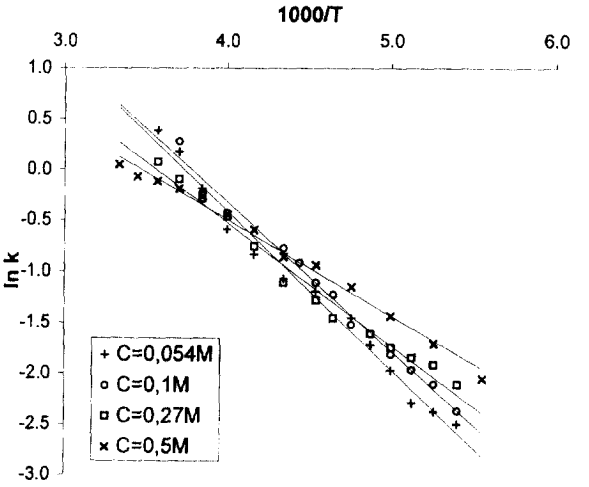

Fig. 4. Arrhenius plots for HS–LS relaxation kinetics in $[Fe(Mepy)_2(Py)tren](ClO_4)_2$ in a series of complexes dissolved in acetone: complex 1: $[Fe(Mepy)_2(py)tren]^{2+}$; 2: $[Fe(Mepy)(Py)_2tren]^{2+}$; and 3: $[Fe(Py)_3tren]^{2+}$.

[2] The idea that Arrhenius type temperature dependencies can result from tunnelling, as it is suggested in the original paper, does not seem probable to us.

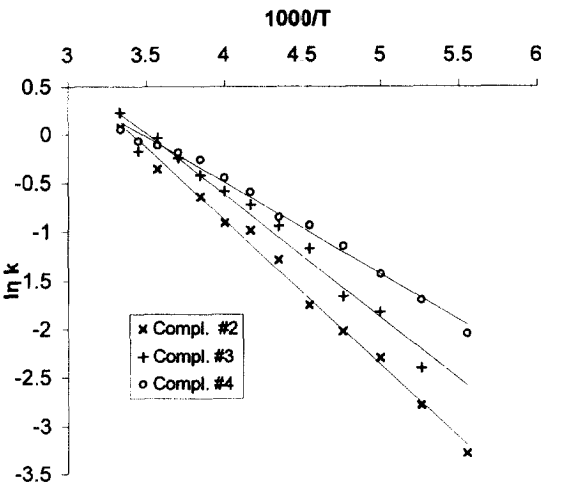

Fig. 5. Arrhenius plots for HS–LS relaxation kinetics in acetone solutions of $[Fe(Py)_3tren](ClO_4)_2$ of varying concentration.

The activation parameters of spin–crossover dynamics of $[Fe(MePy)_2(Py)tren](ClO_4)_2$ have been found to be significantly dependent on the solvent. However, no single mechanism for this influence has been suggested for this influence. Nor do we observe a good IKR in the series of Arrhenius plots with varying solvent[3] (Fig. 6). Solvent effects include both the association and solvation phenomena, therefore, there is no observable IKR. The fact that dilution of

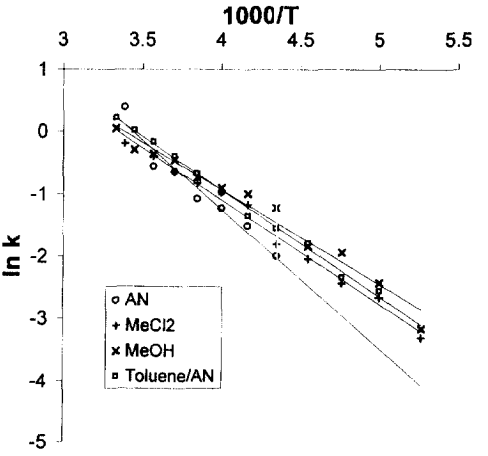

Fig. 6. Arrhenius plots for HS–LS relaxation kinetics in $[Fe(MePy)_2(Py)tren](ClO_4)_2$ dissolved in different solvents.

[3] In fact, leaving one point in the AN series, the general behaviour is isoenthalpic (parallel lines).

Table 1
Activation energies, pre-exponential factors and spin–crossover temperatures in solid and liquid solutions of Schiff base complexes of Fe(III) [46]

Complex	E_a (cm^{-1})	A (s^{-1})	T_{sc} (K)
Fe(III)			
[(In/Fe)Sal_2tr]PF_6	735	3.40×10^{9}	120
[$FeSal_2tr$] in KBr	748	1.80×10^{9}	130
In PN/Bn[a]	1254	4.20×10^{10}	250
In H_2O	1733	8.10×10^{11}	305
In MeOH	1738	1.50×10^{11}	290
In MeOH	1578	2.80×10^{11}	290
Acetone	3301	5.30×10^{15}	280
[$Fe(acpa)_2$]PF_6 in KBr	709	7.00×10^{8}	190
[$Fe(bzpa)_2$]PF_6	880	2.60×10^{8}	220
[$Fe(bzpa)_2$]PF_6 in PN/Bn[a]	1280	4.40×10^{8}	240
Fe(II)			
[(Mn/Fe)pic_3Cl_2]MeOH	1120	2.00×10^{8}	118

[a] Propionitrile/butyronitril.

acetonitrile by toluene brings about a large change in activation energy speaks for the prevailing ion association effects.

In solutions (liquid and solid) of Fe(III) the spin–crossover transition rates are generally significantly higher than in the complexes of Fe(II). A kinetic study [46] of complexes of Fe(III) of different nature and in different matrices shows a correlation between activation energy and the logarithm of pre-exponential factor, yielding an isokinetic temperature of 234 K. This is close to the mean temperature of spin–crossover in this series of 231 K, (see Table 1), which however, must be treated with care as this might be due to statistical artefacts (see Fig. 2).

In solid diluted complexes of Fe(II), the relaxation kinetics is exponential but the temperature dependencies are non-Arrhenius with a considerable contribution from temperature independent tunnelling ($k(T\rightarrow0)$) at low temperatures. This contribution increases with the increasing energy gap between HS and LS states, which reveals itself in the correlation between ln $k(T\rightarrow0)$ and transition temperature (T_{sc}). Kinetic data on various diluted spin–crossover complexes of Fe(II) reported in Ref. [47] are shown in Table 2.

Table 2
Transition temperatures T_{sc}, activation energies E_a, preexponential factors A and low temperature tunnelling rate constants for intersystem crossing rates in some Fe(II) compounds [47]

	T_{sc}(K)	E_a (cm^{-1})	A (s^{-1})	k $(T\rightarrow0)$ (s^{-1})
$[Zn_{1-x}Fe_x(ptz)_6](BF_3)_2$	95	1100	5×10^{7}	$\sim5\times10^{-7}$
$[Mn_{1-x}Fe_x(pic)_6]Cl_2\cdot MeOH$	118	907	2×10^{8}	2.5×10^{-7}
$[Zn_{1-x}Fe_x(mepy)_6](PF_6)_2$	210	837	5×10^{8}	1.4×10^{-7}
$[Zn_{1-x}Fe_x(py)_6](PF_6)_2$	>350	640	1×10^{9}	4×10^{2}
$[Zn_{1-x}Fe_x(bipy)_6](BF_3)_2$	low spin	364	2×10^{9}	6×10^{5}

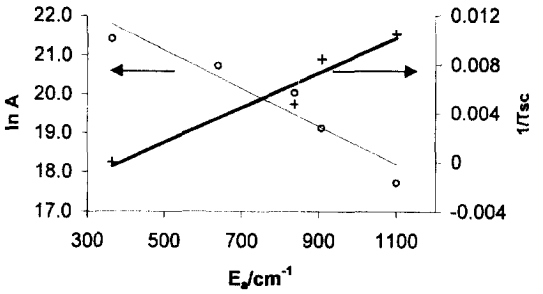

Fig. 7. Correlations between E_a, ln A and inverse temperature of spin–crossover $1/T_{sc}$ for diluted solid spin–crossover complexes shown in Table 2.

These data reveal a well pronounced correlation between ln A and E_a (Fig. 7) yielding an isokinetic temperature of -292 K, i.e. a case of anti-compensation where activation energy and preexponential factor vary in different directions.

For relaxation kinetics in spin–crossover compounds, a certain empirical rule is established called the inverse energy gap rule [3]. According to this rule, the higher the difference in energies of HS and LS states (energy gap), the lower the activation energy of relaxation. If we consider the activation barrier as arising from the intersection of potential energy surfaces, the higher the energy of HS (hence $T_{1/2}$) the lower the potential barrier for relaxation will become (see below, Fig. 19). The frequency of vibrations of a HS state in such a potential well determining the entropic part of activation free energy also decreases. Therefore, the observed negative T_{iso} reflects indirect correlations in this reaction series not connected with the origin of the inverse energy gap law and correlation between E_a and $1/T_{sc}$ (Fig. 7).

In non-diluted solid spin–crossover systems the relaxation from HS to LS state (after the excitation to metastable HS state by light irradiation at low temperatures) is very often non-exponential with a considerable self acceleration due to the interactions between HS centres. Such kinetics can be described by the following equation [48]:

$$\gamma_{HS} = a_0 \exp(-k^0(T) \exp(a(T)(1-\gamma_{HS}))) \tag{3.1}$$

The coefficient $a(T)$ is then responsible for self-acceleration caused by this interaction. Temperature dependencies of the parameters in Eq. (3.1) were determined for a series of solvates: $[Fe(dppen)_2X_2]n$Solv, where $X = Cl^-$ or Br^-, Solv $= CHCl_3$ or CH_2Cl_2 (dppen = diphenylphosphine ethylene). The complex $[Fe(dppen)_2X_2](CHCl_3)_2$ relaxes exponentially ($a(T) = \text{const} = 1$) whilst other complexes show self-acceleration of the relaxation to LS state. Fig. 8 shows 'Arrhenius plots' for k parameters. It is hardly possible to detect anything resembling IKR in these plots. Obviously there are no single parameter variation in these series (i.e. no IKR occurs).

4. Shapes of spin–crossover curves

Spin–crossover compounds are usually crystalline compounds and are often found to be poorly soluble (about 10^{-3} mol l^{-1} and less). Liquid spin–crossover systems are therefore diluted solutions, and the effects of interactions between spin–crossover species are negligible. These systems may therefore be described by the law of mass action of ideal solutions:

$$x_{HS} = (1 - x_{HS})K \tag{4.1}$$

or:

$$\ln((1 - x_{HS})/x_{HS}) = \Delta H_{sc}/RT - \Delta S_{sc}/R \tag{4.2}$$

It is not convenient to use the entropy of spin–crossover, but some other quantity which can be estimated as an approximately independent of ΔH_{sc} parameter. Such a parameter is the temperature of half conversion $T_{1/2}$ or T_{sc} which is connected with the entropy of spin–crossover as follows:

$$\Delta S_{sc} = \Delta H_{sc}/T_{sc} \tag{4.3}$$

The mass action law for spin–crossover can therefore be written as:

$$\ln((1 - x_{HS})/x_{HS}) = (\Delta H_{sc}/R)(1/T - 1/T_{sc}) \tag{4.4}$$

The use of T_{sc} is favoured by a much smaller correlation of the estimates of ΔH_{sc} and T_{sc} than that of the estimates of ΔH_{sc} and ΔS_{sc} when they are determined by regression of experimental data. A typical curve of a gradual spin–crossover described by Eq. (4.4) is shown in Fig. 9.

It must be pointed out that the limiting value of x_{HS} at infinitely high temperatures is not 1 but:

$$x_{HS}\infty = 1/[1 + \exp(-\Delta H_{sc}/RT_{sc})] \tag{4.5}$$

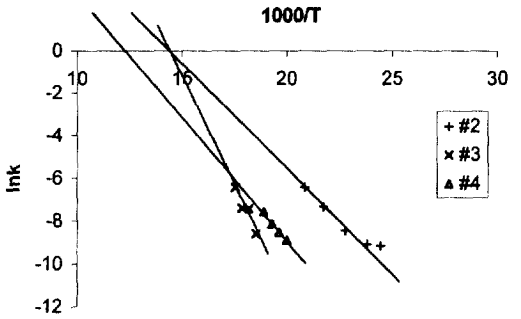

Fig. 8. Temperature dependencies of the rate constant (k) and self acceleration coefficient (a), (Eq. (3.1)), for the HS → LS relaxation kinetics in $[Fe(dppen)_2X_2]Solv_2$: 1: X = Cl, Solv = CH_2Cl_2; 2: X = Br, Solv = $CHCl_3$; and 3: X = Br, Solv = CH_2Cl_2.

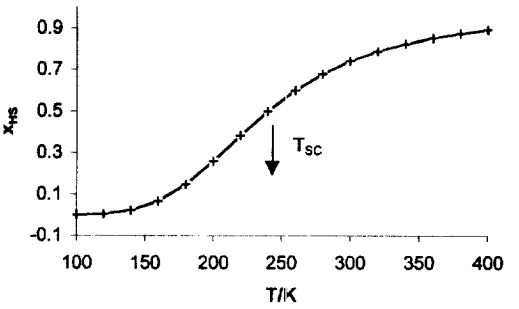

Fig. 9. Simulated spin–crossover curve corresponding to a gradual LS–HS transition ($T_{sc} = 240$ K and $\Delta H_{sc} = 2{,}5$ kcal mol^{-1}).

Therefore the values of μ_{HS} can not be obtained by extrapolating the temperature dependence of μ to infinite temperature. In fact, a nonlinear regression of experimental data to the following system of equations:

$$\mu^2_{obs} = (1 - x_{HS})\mu^2_{LS} + x_{HS}\mu^2_{HS} \tag{4.6}$$

$$x_{HS} = K/(K + 1) \tag{4.7}$$

$$K = \exp(-\Delta H_{sc}/R(1/T - 1/T_{sc}) \tag{4.8}$$

should be used in order to estimate μ_{HS} as well as ΔH_{sc} and T_{sc}. It might be necessary to take the temperature dependence of the magnetic moment of HS state into account, (see Fig. 15) especially if experimental data cover a wide range of temperatures below 200 K. For non-distorted octahedral complexes the temperature dependence of μ_{HS} is given [53] by:

$$\mu^2 = 3\frac{28x + 9.33 + (22.5x + 4.179)e^{-3x} + (24.5x - 13.5)e^{-5x}}{x(7 + 5e^{-3x} + 3e^{-5x})} \tag{4.9}$$

where $x = kT/\lambda$.

The effects of nearest surrounding on the spin–crossover in non-diluted solids are described using regular solutions theory. Under certain simplifying conditions [16,54] free energy of a molecule is dependent on the product of the numbers of the species in equilibrium (A and B):

$$G = \Delta G_{ex} N_A N_B/(N_A + N_B) + N_A G_A + N_B G_B + kTN_A \ln x_A + kTN_B \ln x_B \tag{4.10}$$

where G_A is the Gibbs free energy of the molecule A surrounded by the same molecules A, G_B is the Gibbs free energy of the molecule B surrounded by molecules B, and ΔG_{ex} is the change in free energy upon the simultaneous transfer of molecules A and B from configurations being surrounded by molecules of opposite kind into configurations where they are surrounded by identical molecules. The law of mass action for the spin–crossover may be obtained from the condition $\partial G/\partial x_{HS} = 0$ as:

$$\ln[(1-x_{HS})/x_{HS}] = (1-2x_{HS})\Delta G_{ex}/RT + \Delta F_{SC}/RT$$
$$= [(1-2x_{HS})\Delta G_{ex} + \Delta H_{sc}]/RT - \Delta S_{sc}/R \quad (4.11)$$

This equation predicts a spin–crossover where the slope in the point $x_{HS} = 1/2$ progressively increasing with increasing ΔG_{ex} (Fig. 10). At $\Delta G_{ex} = 2RT$ the slope becomes infinitely high (vertical tangent). At higher values of ΔG_{ex}, the separation of HS and LS phases takes place (similarly to the mixtures of liquids with limited miscibility described by identical equations, [54]). This phase transition leads in many cases to the observation of a hysteresis (not accompanied by the changes in crystal structure).

In the spin–crossover literature, the exchange free energy ΔG_{ex} is called the interaction coefficient (denoted as Γ or γ). The difference in free energies of a molecule in HS state also surrounded by HS molecules and of the same molecule surrounded by LS molecules, proceeds mainly from the mechanical strains originated in different molecular volumes of these states. These strains may be estimated on the basis of a model of defects in continuous elastic media. Hence, the free energy of exchange is interpreted as elastic interaction energy.

As can be seen from Fig. 10(A), Eq. (4.11) predicts an isoequilibrium relationship with $T_{iso} = T_{sc}$ for systems with varying ΔG_{ex}. Such a point of intersection has been observed for the Fe(III) Schiff base complex differently prepared and processed (ground, pressurised etc.) as depicted in Fig. 11, [62]. It is important to note here that dilution (for example with respective Zn(II) complexes) does not refer to the given situation. For an example of such a situation see Fig. 20 and the discussion below.

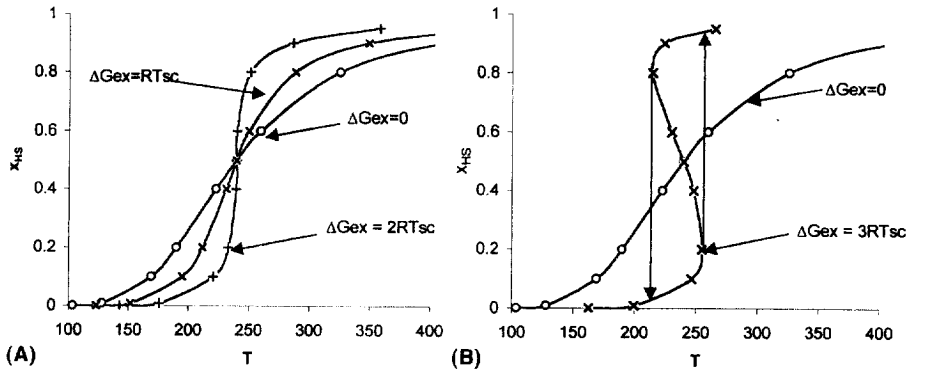

Fig. 10. Shapes of spin–crossover curves. (A) at different values of exchange energy ($\Delta H_{sc} = 2.5$ kcal mol^{-1}, $T_{sc} = 240$ K) and (B) corresponding to the occurrence of hysteresis.

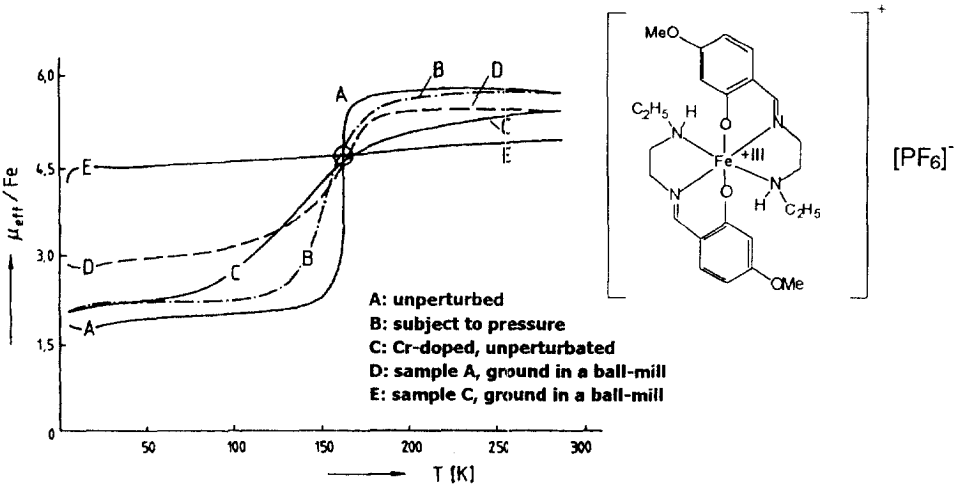

Fig. 11. Spin crossover curves for $Fe(3\text{-}OCH_3\text{-}SalEen)_2PF_6$: A: unperturbed; B: subject to pressure; C: Cr-doped, unperturbed; D: sample A ground in a ball-mill; and E: sample C, ground in a ball-mill [62].

5. Types of spin–crossover curves in series exhibiting isoequilibrium relationship

Usually the data on spin–crossover are represented in the form of temperature dependent observed magnetic moment (μ_{obs}, μ^2_{obs} or χ vs. T) or of the fraction of HS state (x_{HS} vs. T). To investigate possible IERs van't Hoff plots are by far to be preferred. For simplicity we shall consider in the following mainly gradual spin–crossover, which is observed in solutions and diluted solids, because they yield straight van't Hoff lines. However, nonlinear plots might be treated analogously as long as common points of intersection are within, or near the experimental temperature range.

5.1. Compensation

In the case of an IER with a finite and positive T_{iso} value, lying sometimes even within the experimental range of temperatures in a series of spin–crossover equilibria, the variation of ΔH and ΔS compensate each other (Fig. 12). This is commonly associated when speaking about IERs (or IKRs).

5.2. Anticompensation

When isoequilibrium temperature is negative the curves μ_{obs} vs. T do not show any indications of a possible intersection, however, the curves seem to approach each other at higher temperatures. This is even more pronounced in the case of intersection at infinitely high temperature (isoentropic series) (Fig. 13).

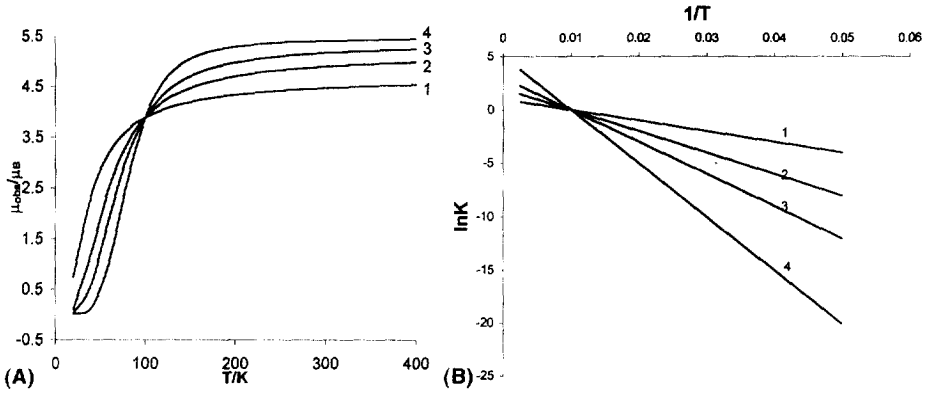

Fig. 12. A series of spin–crossover equilibria exhibiting intersection point (isoequilibrium point) in the range of experimental data (compensation $\delta\Delta H/\delta\Delta S = 100$ K, $\mu_{HS} = 5.5$; 1: $\Delta H/\Delta S = 100/1$; 2: $\Delta H/\Delta S = 200/2$; 3: $\Delta H/\Delta S = 300/3$; and 4: $\Delta H/\Delta 0S = 500/5$): A, μ vs. T curves; B, van't Hoff plots.

5.3. Isoenthalpic reaction series

A series of spin–crossover equilibria without any point of intersection of van't Hoff lines (i.e. parallel lines or an intersection point at $T = 0$ or $1/T = \pm\infty$) would exhibit μ vs. T curves definitely distanced at higher temperatures (Fig. 14). This is the case for the isoenthalpic reaction series.

5.4. Isoentropic reaction series

A series of spin–crossover equilibria with a common point of intersection of the van't Hoff lines at $1/T = 0$ (i.e. infinite temperature) is called isoentropic reaction series (Fig. 15).

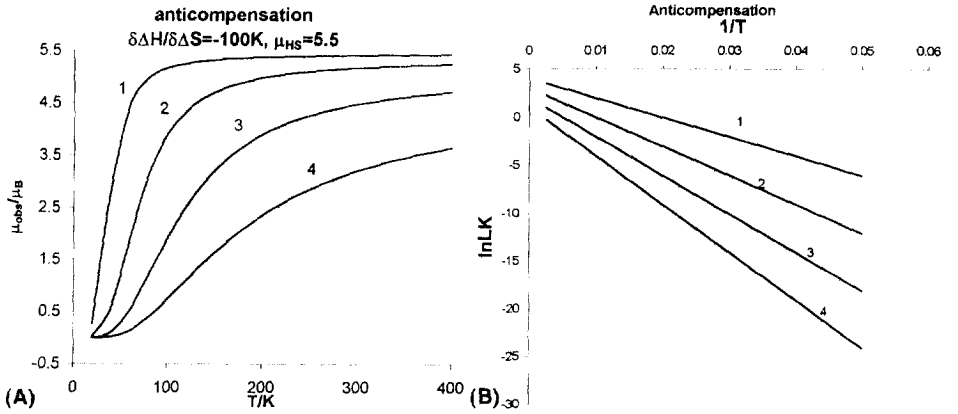

Fig. 13. The case of negative isoequilibrium temperatures (anticompensation: compensation $\delta\Delta H/\delta\Delta S = 100$ K, $\mu_{HS} = 5.5$; 1: $\Delta H/\Delta S = 200/4$; 2: $\Delta H/\Delta S = 300/3$; 3: $\Delta H/\Delta S = 400/2$; and 4: $\Delta H/\Delta S = 500/1$): A, μ vs. T curves; B, van't Hoff plots.

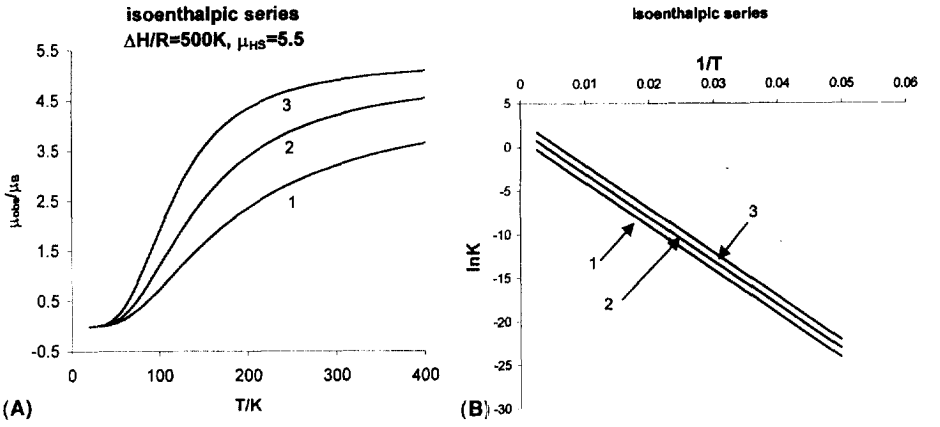

Fig. 14. Isoenthalpic series of spin–crossover equilibria. No intersection point of van't Hoff plots ($\Delta H/R = 500$ K, $\mu_{HS} = 5.5$; 1: $\Delta S/R = 1$; 2: $\Delta S/R = 2$, and 3: $\Delta S/R = 3$): (A) μ vs. T curves; (B) van't Hoff plots.

Not only spin–crossover compounds may show such common points of intersection of the μ vs. T curves. For example, similar behaviour is predicted theoretically [55] for paramagnetic complexes with the ground term $^5T_2$ split in axially distorted octahedral fields (Fig. 16).

The curves μ vs. T corresponding to different distortions of the octahedral crystal field (characterised by the parameter Δ) show a common point of intersection if the ratio Δ/λ is positive (Fig. 16(A)). For negative spin orbit coupling constant λ (more than half-filled d-level: Fe(II)–Cu(II)) this means that the parameter of axial distortion Δ must be also negative. Negative Δ means that corresponding complex exhibits tetragonal compression which is common for octahedral complexes of Fe(II) in the form of dynamic Jan–Teller effect.

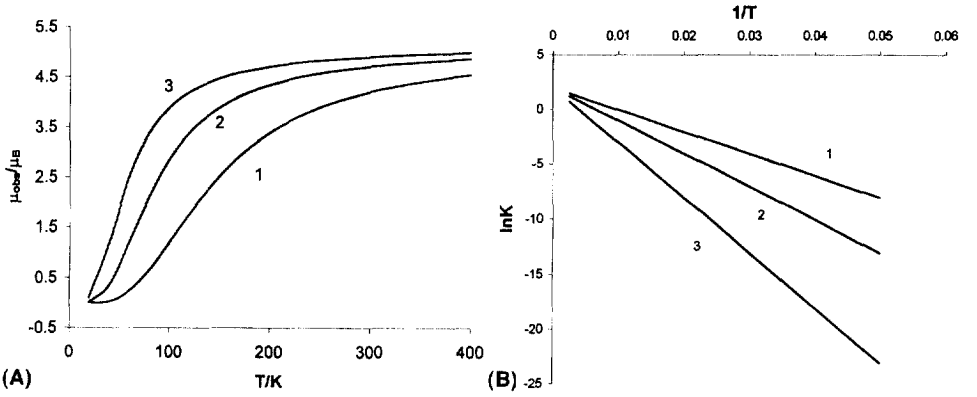

Fig. 15. Isoentropic series of spin–crossover equilibria ($\Delta S/R = 2$, $\mu_{HS} = 5.5$; 1: $\Delta H/R = 500$ K; 2: $\Delta H/R = 300$ K; and 3: $\Delta H/R = 200$ K): A, μ vs. T curves; B, van't Hoff plots.

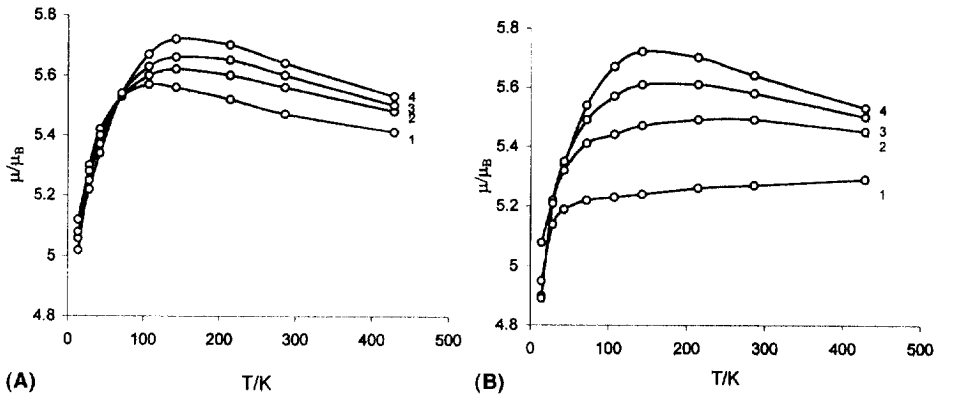

Fig. 16. Temperature dependencies of magnetic moment of the term $^5T_2$ in distorted octahedral crystal field corresponding to $v = \Delta/\lambda = +10$ (1), $+5(2), +3(3)$, 0(4) (A), and $v = \Delta/\lambda = -10(1)$, $-5(2)$, $-3(3)$, 0(4) (B), and the orbital reduction factor $\kappa = 1$.

The common point of intersection of temperature dependence of μ originates in the redistribution (with temperature) of molecules over the sublevels of the term $^5T_2$ in axial fields (Fig. 17). These sublevels have different degeneracy hence provide for a different orbital contribution to magnetic moment.

In the intersection point ($T_{iso} \cong |\lambda/2|/k$, according to Fig. 16(B)), a certain distribution of the populations over the levels of the $^5T_2$ term is achieved, causing the effects of field distortions on the magnetic moments of different multiplets to compensate each other. It must be mentioned that such behaviour is also possible for ions with positive λ (less than half filled d-level: d^1–d^4) and tetragonal elongation.

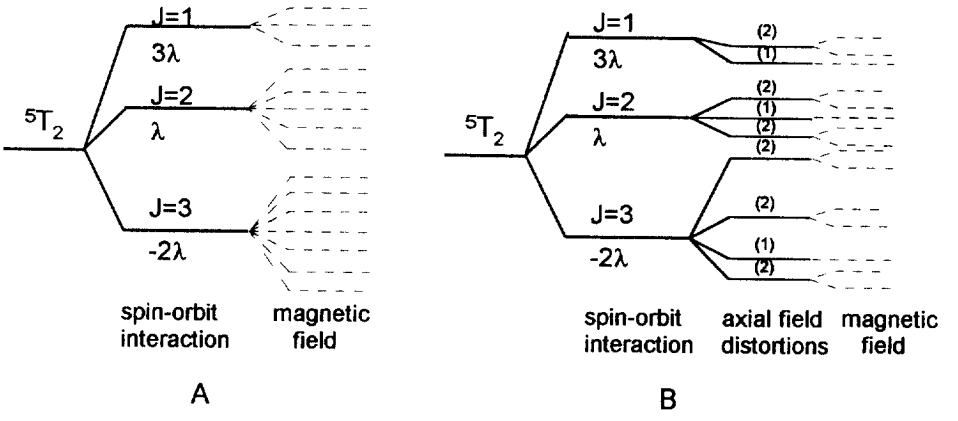

Fig. 17. Splitting of the term $^5T_2$ (corresponding to d^6 configuration) by spin-orbit coupling (A) and axial distortions of octahedral crystal field (B).

The intersection point of temperature dependencies of magnetic moment of axially distorted octahedral complexes having $^5T_2$ ground state, can therefore, be also interpreted as an example of isoequilibrium relationship: it reflects the shifts of equilibria involving molecules with different magnetic moments. From this point of view, the temperature dependence of magnetic moment itself is similar to spin–crossover. However, the spin of particles remain the same, it is the orbital contribution to magnetism (effective orbital momentum) which is different for multiplets. Spin–crossover is also distinguished by a marked change in the bond lengths and must be considered as a pseudo-chemical equilibrium between isomers.

From the material presented above it follows that the curves μ or χT vs. T may not exhibit specific features necessary to detect an IER. In order to identify such behaviour, one has to calculate the equilibrium constant and analyse van't Hoff plots.

However, the calculation of equilibrium constant of a spin–crossover implies that we assume a certain reaction scheme, which might not correspond to the real situation. For example, the complex $[Fe(bzimpy)_2]^{2+}$ in basic and protic solvents exhibit weak acidic properties and an equilibrium exists between protonated and deprotonated species. Thus, spin–crossover occurs between various species characterised by different magnetic moments in HS state, because of different degrees of distortion of octahedral symmetry. The calculation of a single constant of spin–crossover equilibrium in such a situation has no physical significance and results in nonlinear van't Hoff plots with curvature strongly dependent on the choice of μ_{HS} (see below).

6. Spin–crossover and IER in solution

6.1. Tris [2-(2-pyridyl) imidazole] iron(II) complexes

The complexes [(2-(2-pyridyl)imidazole)$_3$Fe](BPh$_4$)$_2$ (**I**) and [(2-(2-pyridyl)-benzimidazole)$_3$Fe](BPh$_4$)$_2$ (**II**) have been found [56] to exhibit spin–crossover in solutions, which yields a good example of an IER.

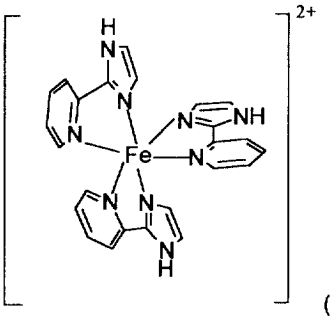

(I)

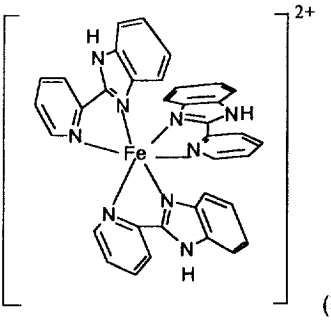

(II)

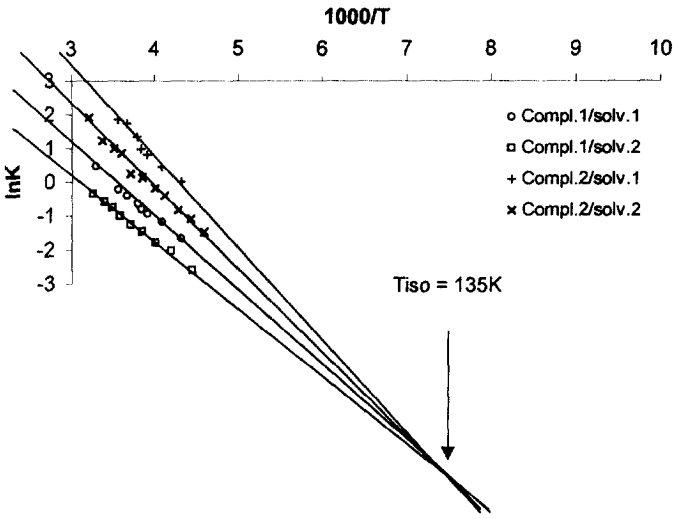

Fig. 18. Isoequilibrium relationship observed in solutions of $[Fe((py)imH)_3](BPh_4)_2$ (complex 1) and $[Fe((Py)bzimH)_3](BPh_4)_2$ (complex 2 in CH_3CN/CH_3OH 1:4 (solvent 1) and acetone (solvent 2).

The van't Hoff plots corresponding to different ligands and different solvents intersect in one point with $T_{iso} = 135$ K (Fig. 18). At this temperature the fraction of HS state is independent of the varying factors (solvents and ligands).

We observe that variation in the structure of ligands and variations in solvents results in the same isoequilibrium temperature, which is rather unexpected because different mechanisms should occur in these series. However, the variation in the structure of the ligands does not affect the configuration of coordinating nitrogen atoms. The addition of a benzene ring to an imidazole unit varies the parameters of spin–crossover equilibrium in the same way as the change in solvation by the used solvents. What parameters determine spin–crossover equilibrium and how their variation may cause an isoequilibrium relationship is considered in the following section.

6.2. Simple statistical model of IER

Equilibrium systems can be understood on the basis of forward and reverse reactions allowing that the theory given above can be applied, provided information about the kinetics for both reactions is available. In case of spin–crossover systems, where both the LS- and HS-states are chemically comparable, T_{iso} of the IER might be calculated (as well as theoretically interpreted) by:

$$T_{iso}^{eq} = \frac{1 - dE_a^f/dE_a^r}{(1/T_{iso}^r - 1/T_{iso}^f)dE_a^f/dE_a^r} \tag{6.1}$$

where T_{iso}^f and T_{iso}^r refer to isokinetic temperatures of forward and reverse reactions, and $E_a^{f,r}$ to the respective activation energies [22]. When HS and LS

states are energetically approximately equivalent so that $E_a^f \cong E_a^r$ i.e. $dE_a^f/dE_a^r = -1$ (ΔH_{SC} is small, which can be found for many examples) this can be simplified by the condition:

$$1/T_{iso}^{eq} \approx (1/T_{iso}^f + 1/T_{iso}^r)/2 \tag{6.2}$$

However, often no information about forward and reverse reaction kinetics is available and an alternative approach to the above given model appears to be necessary.

An IER in a series of spin–crossover equilibria may be explained on the basis of a general statistical mechanical description of chemical equilibrium in condensed phase. In the case of ideal solutions (solid or liquid) the equilibrium constant of spin–crossover:

$$A(LS) \Leftrightarrow B(HS)$$

may be written as:

$$K = x_B/x_A = z_B/z_A \tag{6.3}$$

The partition function z to be used, is the vibrational partition function (the translational partition function is anyway unaffected by spin–crossover) with the contribution from electronic partition function in the form of the degeneracy factor g:

$$z = g^3[e^{-(3/2)h\nu/kT}(1 - e^{-h\nu/kT})^{-3}] \times e^{-\varepsilon_0/kT} = e^{-\varepsilon_0/kT}[g/2sh(h\nu/2kT)]^3 \tag{6.4}$$

Assuming that one mode of vibrations (either intra-molecular or lattice vibrations) contribute significantly to free energy, we use just one vibrational partition function per particle. The equilibrium constant for Eq. (6.3) can then be written as:

$$K = (z_{HS}/z_{LS}) = (g_{HS}/g_{LS})^3 \exp[-(\varepsilon_{0HS} - \varepsilon_{0LS})/kT][sh(h\nu_{LS}/2kT)/sh(h\nu_{HS}/2kT)]^3 \tag{6.5}$$

At ambient and higher temperatures, the vibrational partition function may be approximated as:

$$z = e^{-\varepsilon_0/kT}[gkT/h\nu]^3 \tag{6.6}$$

and the equilibrium constant becomes:

$$K = (z_{HS}/z_{LS}) = (g_{HS}/g_{LS})^3 \exp[-(\varepsilon_{0HS} - \varepsilon_{0LS})/kT][\nu_{LS}/\nu_{HS}]^3 \tag{6.7}$$

The vibrational frequencies ν_i may be estimated for the Lennard–Jones potential (Ref. [54], p. 170) as:

$$\nu = (1/2\pi a_s)\{(2mn|u_s|/3\mu\}^{1/2} \tag{6.8}$$

where μ is the mass of a particle, a_s is the lattice constant, m and n are the exponents in the Lennard–Jones potential, and u_s is the potential energy of a particle at the minimum of potential curve measured (Fig. 19) with respect to zero, i.e. to the potential of a system with infinitely large distances between the particle. It may be identified with the potential energy ε_0 which becomes negative ($\varepsilon_0 = -u$):

$$\ln(z) = 3\ln(g) + 3\ln(kT/hv) - \varepsilon_0/kT$$
$$= 3\ln(g) + (3/2)[\ln(6\pi^2 a^2 kT\mu/mnh^2) - \ln(u/kT)] + u/kT$$
$$= C + 3\ln(g) + (3/2)\ln\mu + 3\ln(a) + (3/2)\ln T - (3/2)\ln(u/kT) + u/kT \quad (6.9)$$

where $C = (3/2)\ln(6\pi^2 k/h^2 mn)$. For $g = 1$, $\mu = \mathrm{M}$ in a.u.m., $m = 6$, $n = 12$ and a in Angstroems:

$$\ln z = -11.619 + (3/2)\ln(\mathrm{MT}) + 3\ln(a) - (3/2)\ln(u/RT)] + u/RT \quad (6.10)$$

For a spin–crossover equilibrium there is no change in the masses of particles and the corresponding equilibrium constant can be written as:

$$\ln K_{\mathrm{SC}} = \ln(z_{\mathrm{HS}}/z_{\mathrm{LS}}) = (U_{\mathrm{HS}} - U_{\mathrm{LS}})/kT - (3/2)\ln(U_{\mathrm{HS}}/U_{\mathrm{LS}}) + 3\ln(g_{\mathrm{HS}}/g_{\mathrm{LS}})$$
$$+ 3\ln(a_{\mathrm{HS}}/a_{\mathrm{LS}}) \quad (6.11)$$

Varying parameters in a reaction series could be either U_{HS}, U_{LS}, or both these quantities. The interatomic distance ratio ($r_{\mathrm{HS}}/r_{\mathrm{LS}}$) can also vary with changing U but its contribution to $\ln K$ must be small, because the whole range of observed variations in a amounts to about 10%. Corresponding change in $3\ln(a_{\mathrm{HS}}/a_{\mathrm{LS}})$ must be about 0.3. The contribution from degeneracy factor normally remains constant and the main variation of $\ln K$ in a reaction series proceeds from the changes in potential energies U.

If only one of these energies is varied in a reaction series there must be a point of intersection of van't Hoff plots, namely with coordinates corresponding to the IER condition:

$$(\partial \ln K/\partial U_i)T_{\mathrm{iso}} = 0 \quad (6.12)$$

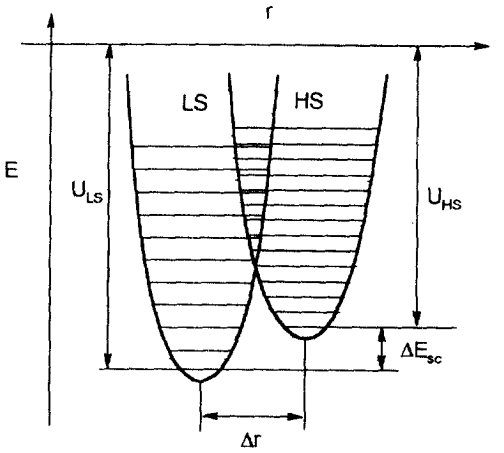

Fig. 19. Potential energies of HS and LS species in a spin–crossover equilibrium (only the lowest vibrational level is shown).

Applying this condition to Eq. (6.11) we get a variation of the high-spin state within the considered reaction series:

$$(\partial \ln K/\partial U_{HS}) = (1/RT_{iso}) - (3/2)(1/U_{HS}) = 0 \tag{6.13}$$

and for a variation of the low spin state:

$$(\partial \ln K/\partial U_{LS}) = -(1/RT_{iso}) + (3/2)(1/U_{LS}) = 0 \tag{6.14}$$

According to Eqs. (6.13) and (6.14), T_{iso} (similarly to IKRs) cannot be negative when either U_{HS} or U_{LS} is varied.

When both these parameters are varied the condition for an IER is:

$$\begin{aligned} d \ln K &= (\partial \ln K/\partial U_{HS})dU_{HS} + (\partial \ln K/\partial U_{LS})dU_{LS} \\ &= (1/RT_{iso})(dU_{HS} - dU_{LS}) - (3/2)[dU_{HS}/U_{HS} - dU_{LS}/U_{LS}] = 0 \end{aligned} \tag{6.15}$$

Special cases occur when the variation is parallel ($dU_{HS} = dU_{LS} = dU$), where no IER condition results because the coefficient at $(1/RT_{iso})$ is zero, as well as in the case of antiparallel variation ($dU_{HS} = dU = -dU_{LS}$) where Eq. (6.15) becomes:

$$dU[(2/RT_{iso}) - (3/2)(1/U_{HS} + 1/U_{LS})] = 0 \tag{6.16}$$

which again shows that T_{iso} is positive. The case of negative T_{iso} corresponds, as already described before, to a system where at least two steps are involved, both of which exhibit independent variations of their characteristic vibrational frequencies, yielding opposite variations of the residual enthalpic and entropic terms (i.e. anticompensation). Another way of visualising this is to imagine the superposition of (at least) two reaction steps (for example solvation followed by spin–crossover, or deprotonation and spin–crossover) with one of them showing an IER with T_{iso} smaller than the mean experimental temperature, the other a T_{iso} higher. In other words, one showing a positive and the other a negative selectivity–reactivity relationship.

According to Eq. (6.13) (i.e. in the case where the energy of HS state alone is varied in a reaction series), the isoequilibrium temperature provides us with an estimate of a characteristic vibrational temperature of the system: The vibrational frequencies entering the expressions for partition functions may be substituted by characteristic temperatures:

$$\theta = h\nu/k \tag{6.17}$$

assuming, based on Einstein' s model crystals, a vibration of uncoupled oscillators yielding Einstein's characteristic temperature. It is not difficult to obtain a relationship between the isoequilibrium temperature of a series of spin–crossover equilibria and characteristic vibrational temperature:

$$\theta = h\nu/k = (h/2\pi ka)(2mnU/3\mu)^{1/2} \tag{6.18}$$

For U expressed in kJ mol^{-1}, μ = reduced mass in a.u.m., $m = 6$, $n = 12$, and a in Angstroems this relationship may be written as:

$$\theta = (1674/a)(U/M)^{1/2} \tag{6.19}$$

or expressing U as a function of θ:

$$U = 3.58 \times 10^{-7}\theta^2 a^2 M \tag{6.20}$$

leading to:

$$T_{iso} = (2/3)U/R = (2/3)3.58 \times 10^{-7}\theta^2 a^2 M/R = 2.37 \times 10^{-7}\theta^2 a^2 M/R \tag{6.21}$$

or:

$$\theta^2 = 4.20 \times 10^6 R T_{iso}/a^2 M \tag{6.22}$$

An example may also be provided from spin–crossover equilibria in solid state (Fig. 20). As mentioned above, a pure spin–crossover complex Fe(II) being diluted with its diamagnetic Zn analogue cannot be considered as the case of varying interaction (exchange) term ΔG_{ex}, which according to Eq. (4.10) would yield an IER with $T_{iso} = T_{sc}$. Fig. 20 shows that this is not the case. The explanation is quite simple: the system contains not just HS and LS species but HS, LS and diamagnetic species, the latter being distinguishable from the LS species of the Fe complex. The configuration entropy will therefore vary for different concentrations, shifting the T_{iso} value to higher temperatures which is reflected in the curves in Fig. 20 with $T_{iso} \cong 150$ K (for $[Fe(2\text{-pic})_3]Cl_2MeOH$ nonlinear van't Hoff lines occur so that T_{iso} has been estimated), $R = 8.314 \times 10^{-3}$ kJ mol^{-1} K. For $a = 8$ Å (estimated minimal distances between Fe-coordination centres) and $\mu = 48.3$ (estimated reduced mass for Fe oscillating within a cage of three 2-pic ligands) we get $\theta \cong 41$ K. This value corresponds to a Debye temperature ($\theta_D = 4/3\theta_E$) of 55 K and can be compared with a Debye temperature of 47.1 K determined [57] for solid $[Fe(2\text{-pic})_3]Cl_2MeOH$ employing the Lamb–Moessbauer factor. It should be mentioned, however, that the Debye temperatures obtained for spin–crossover compounds from Debye–Waller factors are usually in the range 90–150 K [63,64], which would agree with higher T_{iso} values usually estimated from the spin–crossover curves of the respective systems.

7. Changes in reaction mechanism visualised by IKRs and IERs

From the occurrence of a distinct IKR it can generally be concluded that only one reaction mechanism is present for all reactions included in this series. This becomes obvious from the theoretical description in Section 2 where a reaction profile has to be assumed to remain essentially unchanged within the reaction series. In the case where some Arrhenius or van't Hoff plots of the considered reaction series miss the condition of the IKR, or in the case where two or more common points of intersection are found, either a change in the reaction mechanism occurs within the series, or the resonance condition between reactants and their molecular surroundings is not fulfilled. In the case of a substituent variation of the reactants with the reaction performed in one solvent (or on one solid state catalyst) the former must be the case [49–51].

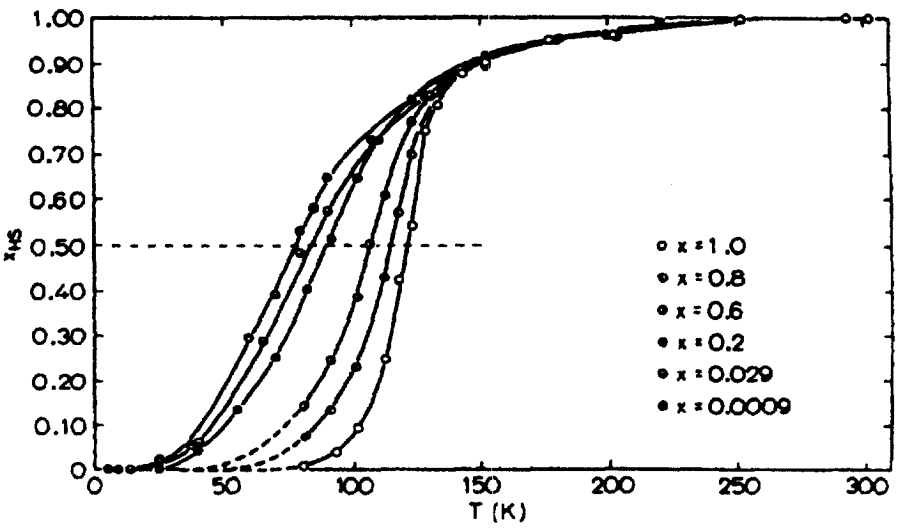

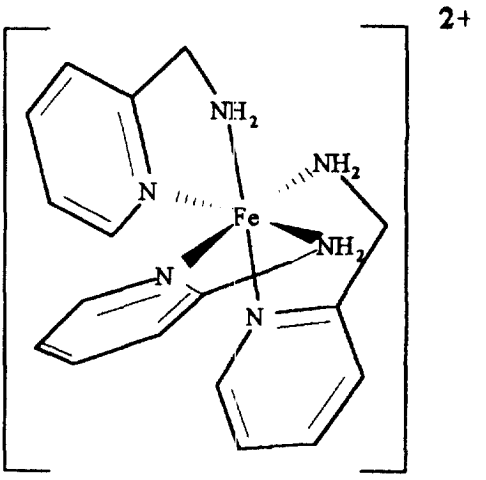

Fig. 20. Temperature dependence of the high-spin fractions measured from the Moessbauer quadruple doublets (x_{HS}) for solid $[Fe_xZn_{x-1}(2-pic)_3]Cl_2 \cdot EtOH$ with a different degree of dilution with Zn^{2+} [65].

The theoretical description given above includes no significant changes in the reaction profile (for example by including a new minimum or maximum according to an intermediate or a new barrier) within one IKR reaction series occur.

Obviously when this is the case, the IKR condition is not fulfilled and more than one common point of intersection may occur. The connections between LFERs discussed above include a similar argument. One IKR can only be found when only one parameter is changed within the reaction series. In the case of a change to the reaction mechanism additional to the parameter describing substituent or solvent variation, other 'information' becomes necessary so that the required condition is not fulfilled. In fact, the IKR analysis has brought to light several, sometimes unexpected, examples of a change in mechanism.

As an example of the applicability of this method to equilibrium systems, we present the study of solvation of square–planar Ni(II) complexes with a diamine and β-diketone as ligands. These complexes are known to show solvatochromism and thermochromism, as well as a change in the spin state due to the equilibrium (Eq. (7.1)):

$$[\text{Ni}(\beta\text{-dike})(\text{diam})]^+ + 2\text{D} \rightleftarrows [\text{Ni}(\beta\text{-dike})(\text{diam})\text{D}_2]^+ \quad (7.1)$$

The influence of the solvent molecules D which are acting as Lewis-bases (i.e. as electron-pair donor molecules) and of different substituents on either of the ligands have been investigated in detail [52], yielding thermodynamic and structural data on the solvent and substituent effects for the transformation of square–planar Ni(II) complexes with a diamine and β-diketone as ligands into octahedrally coordinated species by addition of donor-ligands (mainly donor-solvent molecules). Not unexpectedly, a five-coordinated species appears to be involved in the equilibrium. The charge redistribution depends upon the donor strength of the solvent donor molecule D and leads, in the case of the less symmetric five-coordinated species, to considerable changes to the bond angles (see Fig. 21).

The analysis of temperature dependencies of equilibrium constants revealed two isokinetic groups, namely, one for weaker donor solvents such as acetonitrile, acetone, alcohols etc., and another one including stronger donor-solvents like formamide, *N*,*N*-dimethylformamide, pyridine, dimethylsulphoxide etc. According to the bond angle variation rules, strong donor solvents lead to strong distortion of the planar arrangement of the β-diketonate and the diamine in the case of the five-coordinated species. At the same time, the bond length variations lead to a weakening of the Ni–O bonds at the β-diketonate. Thus, in solvates with strong donor molecules one Ni–O bond is broken, the β-diketonate rotates and a *cis*-configuration results. In weak donor solvents these changes are less pronounced, so that the β-diketonate remains in nearly the same position within the molecule and the second donor-molecule is simply added to form the *trans* isomer. The former reaction path may be described in terms of a dissociative mechanism, whereas the latter may be described in terms of an associative mechanism (see Fig. 22). In fact, X-ray analysis of the solid state octahedral complexes reveals unambiguously the occurrence of the *cis* and *trans* species.

It is interesting that for the CF_3 substituted species only one common point of intersection is found, pointing to the occurrence of only one IKR associated with

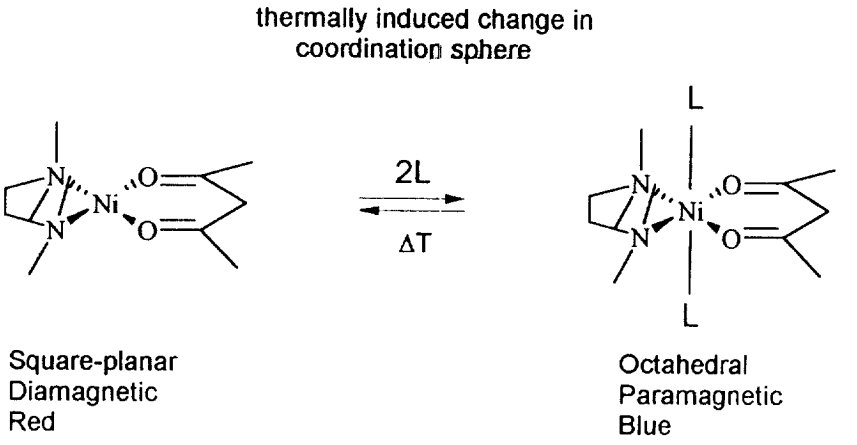

Fig. 21. Solvatochromic mixed ligand complexes of the form Ni(β-diketone)(diamine)+ give an excellent example for investigating temperature dependent equilibrium and kinetics under variation of substituents and reactants. The square–planar species are diamagnetic, octahedral species are paramagnetic.

only one reaction mechanism. However, for these species, the equilibrium constants for both the formation of the five-and the six-coordinated species are, even for the weak donor molecules, much higher than those of the unsubstituted species with strong donor molecules. Therefore, it must be assumed that in this case for all donor solvents the reaction runs via the dissociative mechanism leading to the *cis* species.

The Ni(II)-bis(salicylaldoximato) complex mentioned above builds also adducts with amines. When a solution of this complex in CCl_4 is titrated with an amine, the complex is converted from the square–planar singlet to an octahedral triplet, i.e. a ligand induced pseudo spin–crossover occurs. A series of such equilibria with different amines exhibit an isoequilibrium intersection point at $T_{iso} = 268$ K (Fig. 23), [19b]. Note that van't Hoff's plots are rising which indicate negative enthalpy of transition from LS to HS state.

In conclusion, it may be pointed out that the occurrence of an IKR yield information about the behaviour of a series of reactions: the abscissa position of the associated point of intersection of the van't Hoff or Arrhenius lines refers to the energy exchange between reactants and the surrounding molecular heat bath and one might shed light on the 'physics' of the interaction. The ordinate position of the common point of intersection reflects the 'chemistry' (i.e. the potential profile) of the system, visualising the reactivity as well as the reaction pathway or changes of this within the considered reaction series in case of more than one IKR).

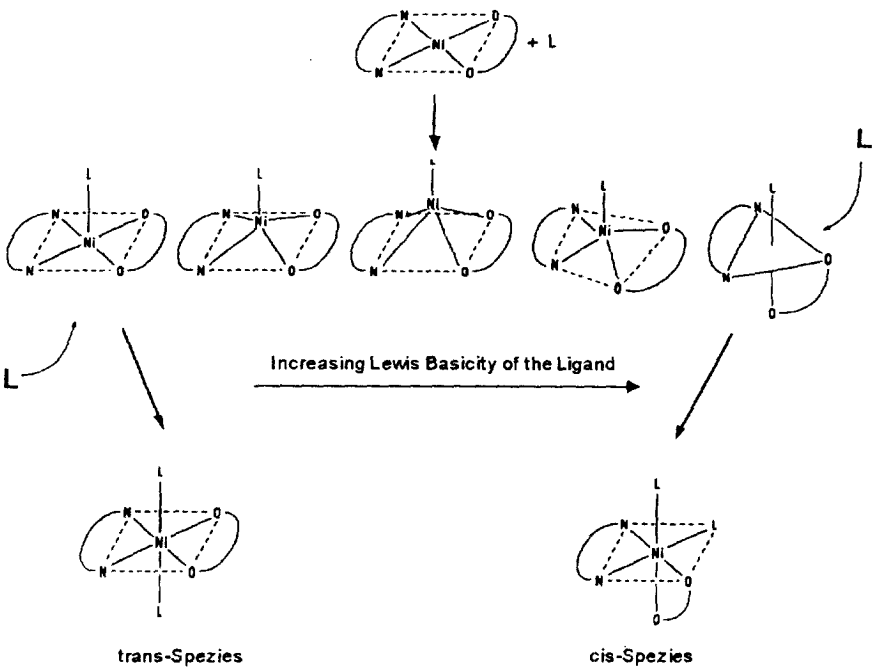

Fig. 22. The formation of octahedral species runs via the formation of a five-coordinated intermediate. The stronger the interaction of the coordination centre with the Lewis-base L, the stronger it is pulled out of the ligand plane, until this distortion flips into a trigonal (distorted) bipyramidal arrangement. The addition of the second L yields *cis* and *trans* species, respectively.

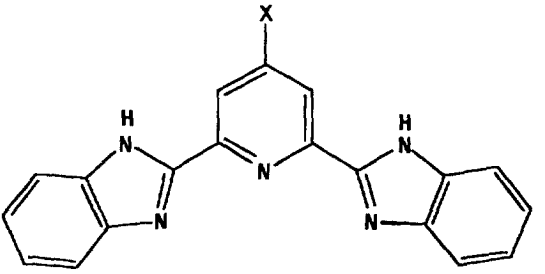

Structure of the Iron(II) complex with **III** is shown below (structure **IV**).

8. The spin–crossover system $[Fe(II)(bzimpy)_2]^{2+}$

Cationic complexes with a series of tridentate ligands, 4-X-2,6-bis-(benzimidazol-2′-yl)-pyridines (III) where X = –H, –OH and –Cl, were isolated as ClO_4^- salts and show thermally induced spin–crossover behaviour ($^1A_1 \rightarrow {}^5T_{2g}$) [58–61].

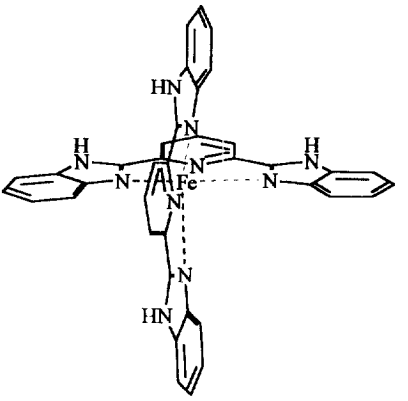

Van't Hoff plots for spin–crossover in this complex have to be investigated, varying substituents and solvents, separately (see Fig. 24). The influence of substituents in the 4th position of the ligand yields a good IER with well defined $T_{iso} = 294$ K for solutions in MeOH (Fig. 24(A)).

However, variation of the solvent of unsubstituted $[Fe(bzimpy)_2]^{2+}$ yields a less good (but still significant) defined IER ($T_{iso} \cong 266$ K (Fig. 24) for aprotic solvents with the results obtained for MeOH being significantly separated. The mechanism of variation of thermodynamic parameters is obviously different in these cases according to the arguments given in Section 7 above.

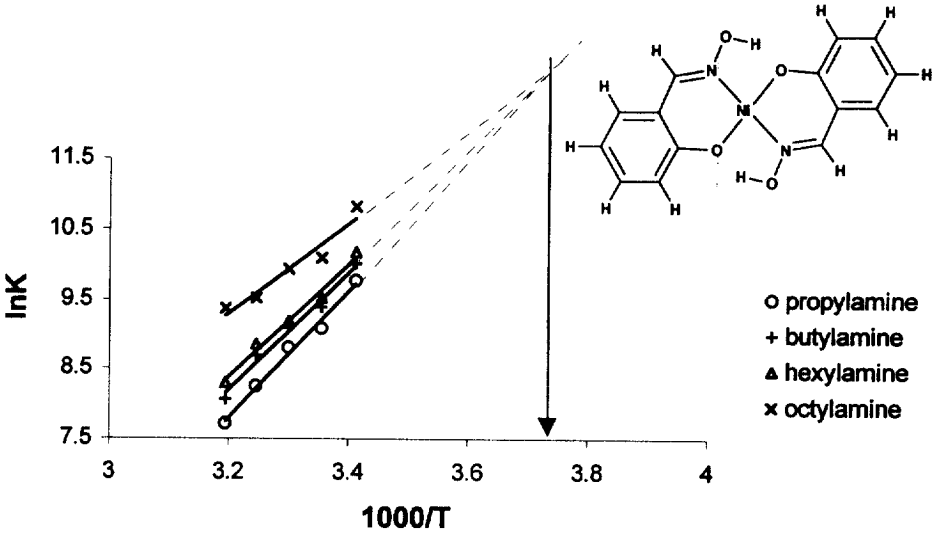

Fig. 23. Isoequilibrium relationship in the series of adducts of bis-(salicylaldoximato)nickel(II) $[Ni(Saldox)_2]$ with amines.

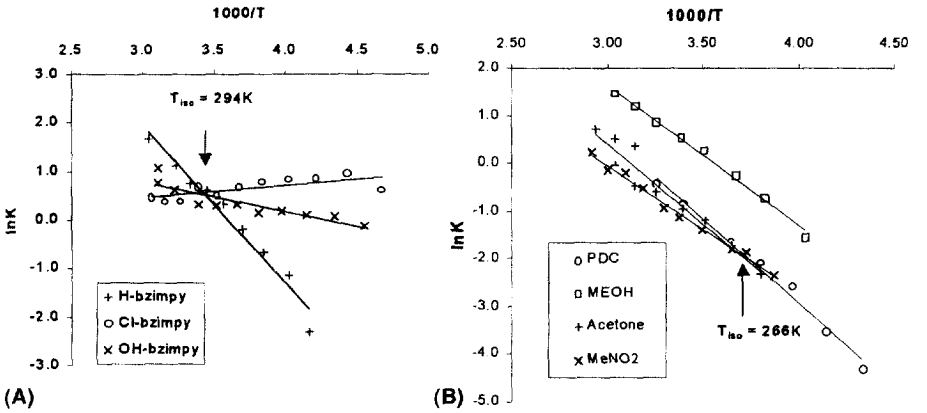

Fig. 24. Van't Hoff plots for spin–crossover in solutions of $[Fe(X\text{-bzimpy})_2](ClO_4)_2$ in the cases of variation of the substituent X (A—in MeOH) and variation of solvent (B—for $[Fe(bzimpy)_2](ClO_4)_2$).

Methanol is a protic solvent and so that $Fe(bzimpy)_2]^{2+}$ behaves as a weak acid [61], therefore, the fact that measurements in MeOH do not meet the common point of intersection of aprotic solvents may be connected with changes in acidic properties of the complexes with different substituents. In the case of aprotic solvents, the variation appears to be simply connected with solvation of this complex and perhaps ligand substitution in the case of DMF (not shown in Fig. 24).

Spin–crossover and effects of substituents are reflected in varying values of magnetic moment of this complex at room temperature. In MeOH solution at 295 K they are:

$$[Fe(bzimpy)_2]^{2+}: \mu_{exp} = 2.50\ \mu_B$$

$$[Fe(OH\text{–}bzimpy)_2]^{2+}: \mu_{exp} = 4.20\ \mu_B$$

$$[Fe(Cl\text{–}bzimpy)_2]^{2+}: \mu_{exp} = 4.30\ \mu_B$$

Of these complexes $[Fe(bzimpy)_2]^{2+}$ alone shows a pronounced spin–crossover in methanolic solutions with magnetic moment varying from 1.30 to 3.40 μ_B in the temperature range 213–328 K, and corresponding changes in UV–vis spectra.

The complex with 4-OH-substituted bzimpy shows smaller variation of magnetic moment with temperature ($\mu_{exp} = 3.77 \rightarrow 4.73\ \mu_B$ at $220 - 332$ K) which suggests an incomplete spin–crossover.

This complex behaviour might be connected with complexation–dissociation equilibria in solution. A generalised reaction scheme describing complex–formation equilibria in solutions of $[Fe(X\text{–}bzimpy)_2]^{2+}$ may be represented as (S = solvent; L = 4-X–bzimpy).

Table 3
Formation constants, absorption maxima of $[FeL_2]^{2+}$, and molar absorptions of $[FeL]^{2+}$ and $[FeL_2]^{2+}$ in methanol at 293 K

Ligand	λ_{max} (nm)	ε_{max} ($dm^3\ mol^{-1}\ cm^{-1}$)	ε_{max} ($dm^3\ mol^{-1}\ cm^{-1}$)	Log K_1	Log K_2
bzimpy	557	350 ± 20	6600 ± 50	5.72 ± 0.05	4.35 ± 0.05
4-OH–bzimpy	515	150 ± 20	1800 ± 20	5.70 ± 0.05	4.44 ± 0.05
4-Cl–bzimpy	500	150 ± 20	1550 ± 20	5.67 ± 0.05	4.38 ± 0.05

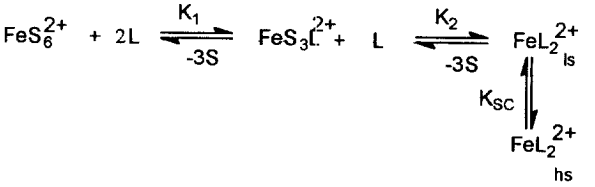

The scheme shows that mono- and bis-complexes are formed in consecutive steps and that the spin–crossover equilibrium occurs in the bis-complexes.

8.1. Complex formation equilibria

At stoichiometric and higher ligand-to-metal ratios (L/Fe = 2.0–20) in MeOH, the UV–vis spectra indicate the formation of the $[FeL_2]^{2+}$ species. At lower ligand-to-metal ratios (L/Fe ≤ 0.5), the peak (at shorter wavelength) associated with an $[FeL]^{2+}$ species, becomes increasingly important. Only these two species are formed in methanolic solutions according to spectrophotometric data on bzimpy, 4-OH–bzimpy, and 4-Cl–bzimpy complexes with Fe(II).

Table 4
Spin–equilibrium constants and thermodynamic parameters of some iron(II)–imine complexes in different solvents

Complexes	Solvent	H (kJ mol^{-1})	S (J $K^{-1}\ mol^{-1}$)	$K_{sc}^{(293)}$	Ref.
$[Fe(bzimpy)_2(ClO_4)_2]$[a]	MeOH	20.51 ± 0.4	58.60 ± 0.4	0.26	[57]
$[Fe(bzimpy)_2(ClO_4)_2]$[a]	DMF/MeOH (20%)	29.43 ± 0.4	93.06 ± 0.4	0.38	[57]
$[Fe(bzimpy)_2(ClO_4)_2]$[a]	NM	20.39 ± 0.4	60.82 ± 0.4	0.36	[57]
$[Fe(bzimpy)_2(ClO_4)_2]$[a]	Ac	22.52 ± 0.4	68.06 ± 0.4	0.39	[57]
$[Fe(bzimpy)_2(ClO_4)_2]$[a]	An	17.37 ± 0.4	57.26 ± 0.4	0.77	[57]
$[Fe(bzimpy)_2(ClO_4)_2]$[a]	PDC	23.90 ± 0.4	73.88 ± 0.4	0.43	[57]
$[Fe(bzimpy)_2(ClO_4)_2]$[b]	MeOH	16.53 ± 1.6	54.21 ± 2.0	0.85	[57]
$[Fe(bzimpy)_2(ClO_4)_2]$[b]	DMF	0.925 ± 0.4	141.1 ± 1.6	0.57	[6]
$[Fe(pybzim)_3(BPh_4)]$[a]	CH_3COCH_3	19.67 ± 0.4	77.86 ± 2.0	3.62	[4]
$[Fe(pybzim)_3(BPh_4)]$[a]	CH_3CN/MeOH(20%)	21.35 ± 1.6	92.09 ± 6.8	10.00	[4]

[a] From magnetic measurement.
[b] From spectroscopic measurement at λ_{max} = 557 nm.

Large log K_1 and log K_2 values (Table 3) in relation to comparable ligands (pyim and bipy)[32,33] confirm that bzimpy is acting as a tridentate ligand in both types of complexes ($[FeL]^{2+}$ and $[FeL_2]^{2+}$). Formation constants are, as expected, little affected by the electron-withdrawing substituents on the ligand.

Thermodynamic parameters of the spin–crossover of $[Fe(H-bzimpy)_2(ClO_4)_2]$ complex in solutions in different solvents were determined using the Evans method and UV–vis spectroscopy (Table 4). Relatively high ΔH_{sc} and ΔS_{sc} values (Table 4) of the complex in 20% (v/v) DMF/MeOH in contrast to that in MeOH, may be attributed to solvation of the imidazole proton which might be expected to stabilise preferentially the LS form: this effect appears to increase with increasing donor number of the solvent.

Returning to Cl- and OH-substituted bzimpy complexes of Fe(II), we must state the magnetic moments 4.0–4.5μ_B for the Cl–bzimpy complex and 3.7–4.7μ_B for the OH–bzimpy complex are less than the pure spin value of a HS state (4, 9 μ_B) and they cannot be attributed to any states with lower multiplicity ($S = 0$ or $S = 1$). The absence of spectroscopic evidence for spin–crossover in these complexes requires some other explanation of the observed variation of magnetic moments. Different degrees of dissociation of a complex could explain such behaviour, but the formation constants are large and approximately equal for all these compounds (Table 3). Another explanation is connected with acidic properties of this ligand and actually of the complex itself.

8.2. Deprotonation of $[Fe(II)(bzimpy)_2]^{2+}$

The NH protons of bzimpy are slightly acidic and they can be abstracted from the molecule by strong bases such as NEt_3. The $[Fe(bzimpy)_2]^{2+}$ behaves in solutions as a weak diprotic acid and when titrated with NEt_3 forms deprotonated species i.e. neutral $[Fe(bzimpyH_{-1})_2]$ which can be isolated as a solid [61]. The acidic properties of bzimpy are affected by substituents, which may be the explanation for different behaviour of Cl- and OH-substituted bzimpy complexes with Fe(II) with respect to non-substituted molecules.

This is illustrated by the pH-dependencies of magnetic behaviour of $[Fe(bzimpy)_2]^{2+}$ in methanolic solutions. In such a system, the value of magnetic moment as a function of temperature and pH can be approximated by the mathematical model based on the simplified reaction scheme.

$$\begin{array}{ccc} & \overset{K_{sc1}}{\rightleftharpoons} & \\ [Fe(LS)[(bzimpy)_2]^{2+} & & [Fe(HS)(bzimpy)_2]^{2+} \\ & \underset{K_{sc2}}{\rightleftharpoons} \quad \overset{K_a}{\rightleftharpoons} & \\ [Fe(LS)[(bzimpyH_{-1})_2] & & [Fe(HS)(bzimpyH_{-1})_2]^{2+} + 2H^+ \end{array}$$

Assuming that the magnetic moment in the low spin state of both species is identical, the expression for the observed in experiment square of magnetic moment may be written as:

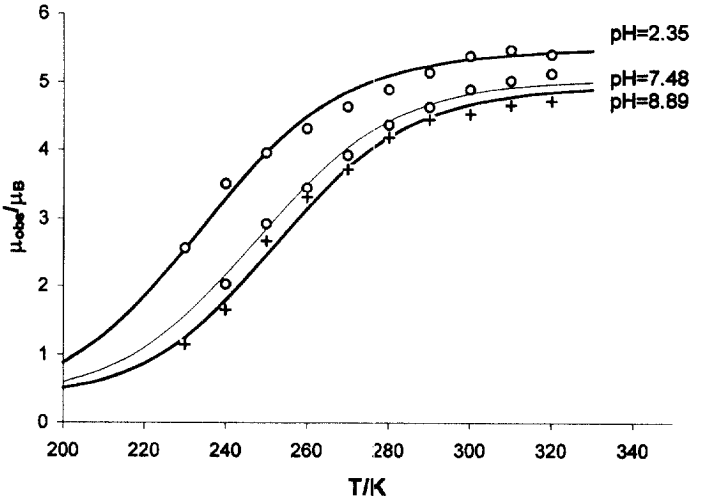

Fig. 25. Temperature dependence of the effective magnetic moment in aqueous methanol solutions of $[Fe(bzimpy)_2](ClO_4)_2$ at different pH. Theoretical curves (lines) are obtained with the same set of parameters shown in Table 5 as corresponding to different pH values.

$$\mu_{obs}^2 = \frac{\mu_{LS}^2\left[1 + \frac{K_a K_{sc1}}{[H]^2 K_{sc2}}\right] + \mu_{HS1}^2 k_{sc1} + \mu_{HS2}^2 \frac{K_a K_{sc1}}{[H]^2}}{1 + K_{sc1}\left(1 + \frac{K_a}{[H]^2}\left(1 + \frac{1}{K_{sc2}}\right)\right)} \tag{8.3}$$

The experimental data (taken from Ref. [66]) show (Fig. 24) that with increasing T, magnetic moment approaches a smaller value in solutions with higher pH. The curves in Fig. 25 are theoretical values calculated according to Eq. (8.3) using parameters shown in Table 5.

The transition temperature for deprotonated species is higher and the magnetic moment in HS state is smaller than those for corresponding parameters of protonated complexes. These differences actually determine the significantly lower effective magnetic moment measured in solutions of $[Fe(bzimpy)_2](ClO_4)_2$ with higher pH. The low magnetic moment of the deprotonated species in the HS state (corresponding to practically pure spin value) results most probably from the lower symmetry of this complex where negative charges are localised on the imidazole

Table 5
Parameters of Eq. (8.3) describing temperature dependence of magnetic moments in the $[Fe(bzimpy)_2]^{2+}$ solutions with different pH

$\Delta H_{sc1}/R$	T_{sc1}/K	$\Delta H_{sc2}/R$	T_{sc2}/K	$\Delta H_a/R$	$\Delta S_a/R$	μ_{LS}/μ_B	μ_{HS1}/μ_B	μ_{HS2}/μ_B	μ_{HSe}/μ_B
4000	249	4800	266	1000	−30	0.45	5.5	4.95	5.5

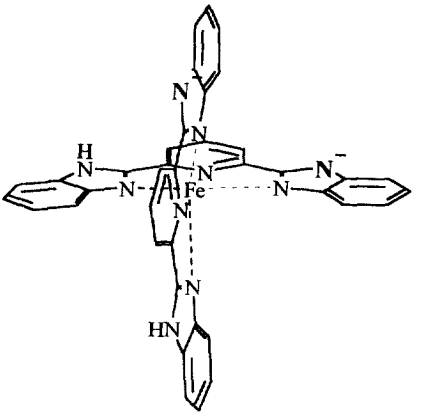

Fig. 26. The localisation of negative charges in the deprotonated [Fe(bzimpyH$_{-1}$)$_2$].

nitrogen atoms (Fig. 26). This cancels the inversion centre symmetry element in the deprotonated complex. In the protonated species, negative charges are localised not on the ligands but on the dissociated counter ions. Therefore, such complexes are of higher symmetry.

8.3. Nonlinear van't Hoff plots of spin–crossover in solution

The experimental data used above can also be analysed [66] by calculating an effective equilibrium constant taking into account just one spin–crossover equilibrium (Eq. (1.6), i.e. not distinguishing between protonated and deprotonated

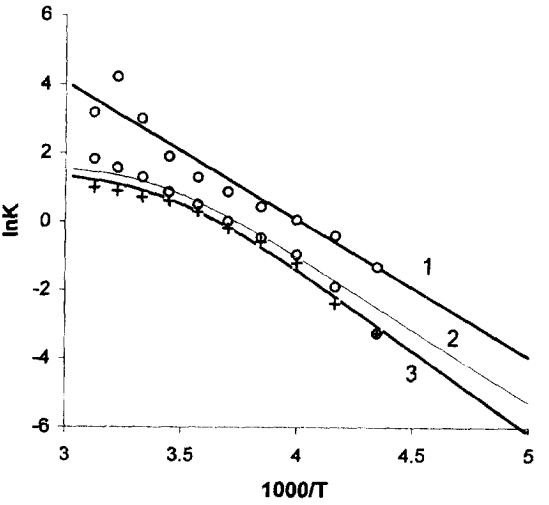

Fig. 27. Van't Hoff plots for spin–crossover of [Fe(bzimpy)$_2$] at different pH (1: pH 2.35; 2: pH 7.48; and 3: pH 8.89) calculated using $\mu_{HS} = 5.5\ \mu_B$.

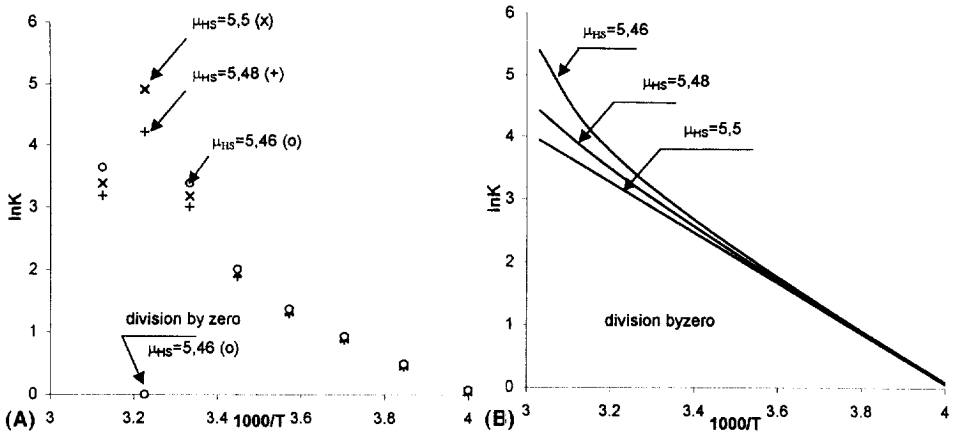

Fig. 28. (A) The effect of different values of μ_{HS} in transformation of μ_{obs} to spin–crossover equilibrium constant (experimental data at pH 2.35), and (B) simulated temperature dependencies of K (Eqs. (1.6) and (8.3)).

species). The resulted van't Hoff plots become nonlinear (Fig. 27) with increasing pH.

This nonlinearity of van't Hoff plots is predicted by the general mathematical model (Eq. (8.3)) and does not require an introduction of the elements of non-ideal solution thermodynamics such as ΔG_{ex}, (Eqs. (4.10) and (4.11)) or a cooperativity term [67]. Theoretical van't Hoff plots (lines in Fig. 27) calculated using Eqs. (8.3) and (1.6) are curved in the region of higher temperature and at higher pH.

Furthermore, the shape of both experimental and theoretical curves depends on the choice of the value of magnetic moment of the HS state (Eq. (1.6)). Theoretical curves given in Fig. 27 have been calculated using the highest values corresponding to the magnetic moment of protonated species (which is an arbitrary choice but produces the least amount of artefacts). Fig. 28 shows what kind of artefacts may be expected when equilibrium constants are calculated using arbitrary values for μ_{HS}.

In calculations based on Eq. (1.6) we are not allowed to use some average value between μ_{HS2} and μ_{HS1} because this would result (at certain temperatures) in infinite or negative equilibrium constants. In general, when the observed magnetic moment approaches the chosen μ_{HS}, the error of calculation K increases very sharply. Therefore, the experimental ln K values show large deviations in the high temperature region of van't Hoff plots (Fig. 28). One point actually corresponding to infinitely high K is represented as zero by the plotting program.

Theoretical van't Hoff plots (Fig. 28) calculated for the system described above take into account that μ_{obs} cannot be higher or equal to μ_{HS}. However, the approximation of a system of equilibria by one spin–crossover equilibrium, results in a positive curvature of van't Hoff plots. We see that experimental points in the region where they are independent of the choice of μ_{HS} also show similar curvature. Such effects do not require for their explanation, any additional assumptions for example, the introduction of an interaction term.

This example shows that in the cases of a spin–crossover accompanied by other reactions, the full system of equilibria should be used in the analysis of experimental temperature dependencies of magnetic susceptibility. In this case, the data on μ_{obs} should be fitted to a theoretical model rather than the van't Hoff plots for an effective spin–crossover equilibrium avoiding the use of arbitrary values of μ_{HS}.

It must be mentioned that all these artefacts only concern the van't Hoff plots based on magnetochemical data. Neither Moessbauer nor UV–vis or IR and Far-IR data would show such behaviour. Therefore, magnetochemical measurements, which are necessary in order to establish qualitatively the presence of a spin–crossover, should be used with caution for quantitative purposes. Moessbauer data for solid state and UV–vis spectra for solutions could be preferable for such measurements.

9. Conclusions

Both IEKs and IERs may occur in spin–crossover transitions as well as in common chemical reactions. These effects provide us with diverse information about the investigated systems and especiallyabout the mechanisms of variations in reaction series. This can be equally important for theoretical studies of spin–crossover transitions and for applied research in this field. We hope that further studies of spin–crossover kinetics and equilibria will supply the material for further IKR and IER analysis.

Acknowledgements

Thanks are due to the Austrian Science Foundation (Project 11218-CHE and 101218-CHE) and to the Training and Mobility of Researchers Network (TMR) project Thermal and Optical Spin State Switching (TOSS) supported by the European Community under the Contract number ERB-FMRX-CT98-0199) and to the European Science Foundation under the project Molecular Magnets.

References

[1] P. Guetlich, A. Hauser, H. Spiering, Angew. Chem. Int. Ed. 33 (1994) 2024.
[2] O. Kahn, Molecular Magnetism, VCH, New York, 1993.
[3] P. Guetlich, A. Hauser, Coord. Chem. Rev. 97 (1990) 1.
[4] H. Toftlund, Coord. Chem. Rev. 94 (1989) 67.
[5] K. Madeja, E. König, J. Inorg. Nucl. Chem. 25 (1963) 377.
[6] L. Cambi, L. Szego, Ber. Dtsch. Chem. Ges. B 64 (1931) 259.
[7] M.A. Hoselton, L.J. Wilson, R.S. Drago, J. Am. Chem. Soc. 97 (1975) 1722.
[8] K.A. Reeder, E.V. Dose, L. Wilson, Inorg. Chem. 17 (1978) 1071.
[9] M.G. Simmons, L.J. Wilson, Inorg. Chem. 16 (1977) 126.
[10] A.W. Addison, S. Burman, C.G. Wahlgren, O.A. Rajan, T.M. Rowe, E. Sinn, J. Chem. Soc. Dalton Trans. (1987) 2621.

[11] J.P. Jesson, S. Trofimenko, D.R. Eaton, J. Am. Chem. Soc. 89 (1967) 3158.
[12] D.M.L. Goodgame, A.A.S.C. Machado, Inorg. Chem. 8 (1969) 2031.
[13] B. Strauß, W. Linert, V. Gutmann, R.F. Jameson, Monatsh. Chem. 123 (1992) 537.
[14] (a) B. Strauß, V. Gutmann, W.Linert, Monatsh. Chem. 124 (1992) 391. (b) B. Strauß, V. Gutmann, W.Linert, Monatsh. Chem. 124 (1992) 515.
[15] H. Li Chum, J.A. Vanin, M.I.D. Holanda, Inorg. Chem. 21 (1982) 1146.
[16] A.B. Koudriavtsev, Chem. Phys. (1999), in press.
[17] R. Jakobi, H. Spiering, P. Guetlich, J. Phys. Chem. Solids 53 (1992) 267.
[18] R.H. Holm, Inorg. Chem. 2 (1969) 307.
[19] (a) A.B. Kudryavtsev, G. Frauendienst, W. Linert, J. Coord. Chem. 46 (1998) 221. (b) G. Frauendienst, Thesis, Vienna, 1997.
[20] A. Taha, W. Linert, Y. Fukuda, J. Coord. Chem. 30 (1993) 53.
[21] W. Linert, A. Taha, J. Chem. Soc. Dalton Trans. 1091 (1994).
[22] W. Linert, Chem. Phys. 114 (1987) 457.
[23] W. Linert, R.F. Jameson, Chem. Soc. Rev. 18 (1989) 477.
[24] W. Linert, J. Chem. Inf. Comp. Sci. 32 (1992) 221.
[25] W. Linert, Chem. Soc. Rev. 23 (1994) 430.
[26] L.P. Hammett, Physikalische Organische Chemie, Verlag Chemie, Weinheim, 1973.
[27] J.N. Brønsted, Chem. Rev. 5 (1929) 238.
[28] (a) V. Gutmann, The Donor–Acceptor Approach to Molecular Interactions, Plenum Press, New York, 1978. (b) W. Linert, V. Gutmann, Coord. Chem. Rev. 117 (1992) 159.
[29] C. Reichardt, Solvent Effects in Organic Chemistry, Verlag Chemie, Weinheim, 1979.
[30] J.E. Leffler, E. Grunwald, Rates and Equilibria of Organic Reactions, Wiley, New York, 1963.
[31] R.P. Wells, Linear Free Energy Relationships, Academic Press, New York, 1968.
[32] W. Linert, R.F. Jameson, Chem. Soc. Rev. 18 (1989) 477.
[33] W. Linert, Inorg. Chim. Acta 141 (1988) 223.
[34] H.A. Kramers, J. Catal. 78 (1982) 238.
[35] (a) B.J. McCoy, R.G. Carbonell, Chem. Phys. 20 (1977) 227. (b) B.J. McCoy, R.G. Carbonell, J. Chem. Phys. 66 (1977) 4564.
[36] I. Oppenheimer, K.E. Schuler, G.E. Weiss, Adv. Mol. Relax. Process. 1 (1967) 13.
[37] R.N. Schwartz, Z.I. Slavsky, K.F. Herzfeld, J. Chem. Phys. 20 (1952) 1591.
[38] W. Linert, J. Chem. Phys. 116 (1987) 381.
[39] L. Landau, E. Teller, Phys. Z. Soviet Union 40 (1936) 34.
[40] W. Linert, Chem. Phys. 129 (1989) 381.
[41] W. Linert, A.B. Kudryavtsev, R. Schmid, Aust. J. Chem. 36 (1983) 1903.
[42] W. Linert, Aust. J. Chem. 38 (1985) 677. (b) W. Linert, Aust. J. Chem. 39 (1986) 199.
[43] W. Linert, V.N. Sapunov, Chem. Phys. 119 (1988) 265.
[44] A.J. Conti, C.-L. Xie, D.N. Hendrickson, J. Am. Chem. Soc. 111 (1989) 1171.
[45] K.F. Purcell, J. Am. Chem. Soc. 101 (1979) 5147.
[46] S. Schenker, A. Hauser, R.M. Dyson, Inorg. Chem. 35 (1996) 4676.
[47] A. Hauser, A. Vef, P. Adler, J. Chem. Phys. 95 (1991) 8710.
[48] C.C. Wu, S. Jung, P.K. Gantzel, P. Gütlich, D.N Hendrikson, Inorg. Chem. 36 (1997) 5339.
[49] W. Linert, V.N. Sapunov, Chem. Phys. 119 (1988) 265.
[50] W. Linert, Aust. J. Chem. 39 (1986) 199.
[51] W. Linert, J. Chem. Phys. 116 (1987) 381.
[52] A. Taha, V. Gutmann, W. Linert, Monatsh. Chem. 122 (1991) 327.
[53] V.T. Kalinnikov, Yu.V. Rakitin, Vvedenie v magnetokhimiyu, Moskva, 'Nauka', 1980 p. 171.
[54] E.A. Moelwyn-Hughes, Physikalische Chemie, 'Thieme', Stuttgart, 1970 p. 427.
[55] B.N. Figgis, J. Lewis, F.E. Mabbs, G.A. Webb, J. Chem. Soc. A (1967) 442.
[56] K.A. Reeder, E.V. Dose, L.J. Wilson, Inorg. Chem. 17 (1978) 1071.
[57] P. Adler, L. Wiehl, E. Meissner, C.P. Koehler, H. Spiering, P. Guetlich, J. Phys. Chem. Solids 48 (1987) 517.
[58] W. Linert, M. Konecny, F. Renz, J. Chem. Soc. Dalton Trans. (1994) 1523.
[59] (a) M. Enamulla, W. Linert, J. Coord. Chem. 35 (1995) 325. (b) M. Enamulla, W. Linert, J. Coord. Chem. 38 (1996) 337. (c) M. Enamulla, W. Linert, J. Coord. Chem. 40 (1996) 193.

[60] M. Enamullah, F. Renz, U. El-Ayan, G. Wiesinger, W. Linert, Vibr. Spectrosc. 14 (1997) 95.
[61] A.W. Addison, S. Burman, C.G. Waehlgren, O.A. Rajan, T.M. Bowe, E. Sinn, J. Chem. Soc. Dalton. Trans. (1987) 2621.
[62] M.S. Haddad, M.W. Lynch, W.D. Federer, D.N. Hendrickson, Inorg. Chem. 20 (1981) 131.
[63] J.A. Real, H. Bolvin, A. Bousseksou, A. Dvorkin, O. Kahn, F. Varret, J. Zarembowitch, J. Am. Chem. Soc. 114 (1992) 4650.
[64] H.-R. Chang, J.K. MacCusker, H. Toftlund, S.R. Wilson, A.X. Trautwein, H. Winkler, D.N. Hendrickson, J. Am. Chem. Soc. 112 (1990) 6814.
[65] M. Sorai, J. Ensling, P. Gütlich, Chem. Phys. 17 (1978) 2509.
[66] (a) F. Renz, Thesis, Vienna, 1997. (b) F. Renz et al., in press.
[67] (a) R. Boca, P. Baran, L. Dihán, H. Fuess, W. Haase, W. Linert, F. Renz, I. Svoboda, F. Werner, Inorg. Chim. Acta 260 (1997) 129. (b) F. Renz, Thesis, Tech. Univ. Vienna, 1997.